RESEARCH ARTICLE

Running head: Plasma membrane lipids in tobacco

Corresponding author:
Sébastien Mongrand
Laboratoire de Biogenèse Membranaire (LBM), UMR 5200, CNRS-University of Bordeaux, 71 avenue Edouard Bourlaux, 33883 Villenave d'Ornon Cedex, France
Tel: 033 663266000
Fax 033 5 56 51 83 61
e-mail: sebastien.mongrand@biomemb.u-bordeaux2.fr

Research Area:
Membranes, Transport and Biogenetics: Associate Editor Anna Amtmann (Glasgow)

Secondary Research Area:
Biochemistry and Metabolism: Associate Editor Julian Hibberd (Cambridge) and Cathie Martin (Norwich)

RE-VISITING PLANT PLASMA MEMBRANE LIPIDS IN TOBACCO: A FOCUS ON SPHINGOLIPIDS

Jean-Luc Cacas[1,3], Corinne Buré[2], Kevin Grosjean[3], Patricia Gerbeau-Pissot[3], Jeannine Lherminier[4], Yoann Rombouts[5,6], Emmanuel Maes[5,6], Claire Bossard[1,7], Julien Gronnier[1], Fabienne Furt[1], Laetitia Fouillen[1], Véronique Germain[1], Emmanuelle Bayer[1], Stéphanie Cluzet[8], Franck Robert[4], Jean-Marie Schmitter[2], Magali Deleu[7], Laurence Lins[7], Françoise Simon-Plas[4], Sébastien Mongrand[1]

[1,] Laboratoire de Biogenèse Membranaire (LBM), CNRS-University of Bordeaux, UMR 5200. 71 avenue Edouard Bourlaux, F-33883 Villenave d'Ornon Cedex, France

[2,] Chimie Biologie des Membranes et Nanoobjets CBMN - UMR 5248 Centre de Génomique Fonctionnelle BP 68 Université de Bordeaux. 146, rue Léo Saignat F-33076 Bordeaux Cedex, France

[3,] Université de Bourgogne UMR1347 Agroécologie, ERL 6300 CNRS, 17 Rue Sully, BP 86510, F-21065 Dijon Cedex, France

[4,] INRA UMR1347 Agroécologie, ERL 6300 CNRS, 17 Rue Sully, BP 86510, F-21065 Dijon Cedex, France

[5,] Université de Lille 1, Unité de Glycobiologie Structurale et Fonctionnelle, Villeneuve d'Ascq, France

[6,] CNRS, UMR 8576, Villeneuve d'Ascq, France

[7,] Laboratoire de Biophysique Moléculaire aux Interfaces (LBMI), Université de Liège, 2, Passage des Déportés, B-5030 Gembloux, Belgium

[8,] ISVV, Groupe d'Etude des Substances Végétales à Activité Biologique (GESVAB), University of Bordeaux, EA 3675, F-33140 Villenave-d'Ornon, 3 avenue Espeleta, F-33400 Talence, France

One-sentence summaries:

This paper shows that GIPCs are major lipids of the PM forming raft in the outer leaflet, yet extending into the inner one through VLCFA, thereby creating interdigitation across the membrane.

FOOTNOTES

Financial source:

We acknowledge the French Agence Nationale de la Recherche (ANR), programme blanc "PANACEA" NT09_517917, contracts to SM and FSP. Lipidomic analyses were performed on Bordeaux Metabolome Facility-MetaboHUB (ANR-11-INBS-0010), contracts to SM and LF (http://www.biomemb.cnrs.fr/page_8.html). JLC was supported by ANR projet blanc "PANACEA" NT09_517917. SM, LF, MD and LL are supported by the ARC FIELD project "Finding Interesting Elicitor LipiDs", and financial support of FSR, University of Liege. MD and LL thank the Belgian Funds for Scientific Research (FNRS) for their position as Senior Research Associate. Financial support from the TGIR-RMN-THC Fr3050 CNRS for conducting the research is gratefully acknowledged.

Present address:

FF, Worcester Polytechnic Institute, Department of Biology and Biotechnology, 100 Institute Road, Worcester, MA 01609, USA

ABSTRACT

Lipid composition of plasma membrane (PM) and the corresponding Detergent-Insoluble Membrane (DIM) fraction were analyzed with a specific focus on highly polar sphingolipids so-called Glycosyl-Inositol-Phosphoryl-Ceramides (GIPCs). Using tobacco Bright Yellow-2 cell suspension and tobacco leaves (*Nicotiana tabacum*), evidences were provided that GIPCs represent up to 40 mol% of the PM lipids. Comparative analysis of DIMs with the PM showed an enrichment of 2-hydroxylated Very Long Chain Fatty Acid (VLCFA)-containing GIPCs and polyglycosylated GIPCs in the DIMs. Purified antibodies raised against these GIPCs were further used for immunogold-electron microscopy strategy, revealing the distribution of polyglycosylated GIPCs in domains of 35±7nm in the plane of the PM. Biophysical studies also showed strong interactions between GIPCs and sterols, and suggested a role for VLCFA in the interdigitation between the two PM composing-monolayers. The ins and outs of lipid asymmetry, raft formation and interdigitation in plant membrane biology are finally discussed.

INTRODUCTION

Eukaryotic Plasma Membranes (PMs) are composed of three main classes of lipids: glycerolipids, sphingolipids and sterols, which may account for up to 100,000 different molecular species (Yetukuri et al., 2008); (Shevchenko and Simons, 2010). Overall, all glycerolipids share the same molecular moieties in plants, animals and fungi. By contrast, sterols and sphingolipids are different and specific to each kingdom. For instance, the plant PM contain an important number of sterols among which β-sitosterol, stigmasterol and campesterol predominate (Furt et al., 2011). In addition to free sterols, phytosterols can be conjugated to form Steryl Glycosides (SG) and Acyl Steryl Glycosides (ASG) that represent up to ca. 15% of the tobacco PM (Furt et al., 2010). As for sphingolipids, sphingomyelin (SM) the major phospho-sphingolipid in animals, which harbors a phosphocholine as polar head, is not detected in plants. Glycosyl Inositol PhosphorylCeramides (GIPCs) are the major class of sphingolipids in plants, but they are absent in animals (Sperling and Heinz, 2003; Pata et al., 2010). Sphingolipidomic approaches identified up to 200 plant sphingolipids (reviewed in (Pata et al., 2010) and (Cacas et al., 2013).

Although GIPCs belong to one of the earliest classes of plant sphingolipids that have been identified in the late 50's (Carter et al., 1958), only a few GIPCs were structurally characterized to date because of their high polarity, and a limited solubility in typical lipid extraction solvents. For these reasons, they were systematically omitted from published plant PM lipid composition. GIPCs are formed by addition of an inositol phosphate to the ceramide moiety, the inositol head group of which can then undergo several glycosylation steps. The dominant glycan structure, composed of a Hexose-Glucuronic acid (GlcA) linked to the inositol, is called series A. Polar heads containing 3 to 7 sugars, so-called series B to F, have been identified and appeared to be species specific (Bure et al., 2011);(Cacas et al., 2013) (Mortimer et al., 2013). The ceramide moiety of GIPCs consists of a long chain base (LCB), mainly t18:0 (called phytosphingosine) or t18:1 compounds (for review, see (Pata et al., 2010) to which is amidified a very long chain fatty acid (VLCFA); the latter of which being mostly 2-hydroxylated (hVLCFA) with odd or even number of carbon atoms. In plants, little is known about the subcellular localization of GIPCs. It is, however, assumed that they

would be highly represented in PM (Worrall et al., 2003; Lynch & Dunn, 2004; Sperling et al., 2005) even if this remains to be experimentally proven. The main argument supporting such an assumption is the strong enrichment of tri-hydroxylated LCB (t18:n) in DIM fractions (Borner et al., 2005); (Lefebvre et al., 2007), LCB known to be predominant in GIPC's core structure as aforementioned.

In addition to this chemical complexity, lipids are not evenly distributed within the PM. Sphingolipids and sterols can preferentially interact with each other and segregate to form microdomains dubbed membrane raft (Simons and Toomre, 2000). The "membrane raft" hypothesis suggests that lipids play a regulatory role in mediating protein clustering within the bilayer by undergoing phase separation into liquid-disordered (Ld) and liquid-ordered (Lo) phases. The Lo phase, termed membrane raft, was described as enriched in sterol and saturated sphingolipids, and is characterized by tight lipid packing. Proteins, which have differential affinities for each phase, may become enriched in, or excluded from, the Lo phase domains to optimize the rate of protein-protein interactions and maximize signaling processes. In animals, rafts have been implicated in a huge range of cellular processes, such as hormone signaling, membrane trafficking in polarized epithelial cells, T cell activation, cell migration, life cycle of influenza and HIV viruses (Simons and Gerl, 2010) (Simons and Ikonen, 1997). In plants, evidence are raising that rafts are also involved in signal transduction processes and membrane trafficking (reviewed in (Simon-Plas et al., 2011); (Cacas et al., 2012b); (Mongrand et al., 2010).

Moreover, lipids are not evenly distributed between the two leaflets of the PM either. Within PM of eukaryotic cells, sphingolipids are primarily located in the outer monolayer whereas unsaturated phospholipids are predominantly exposed on the cytosolic leaflet. This asymmetrical distribution has been well established in human red blood cells, in which the outer leaflet contains SM, phosphatidylcholine (PC) and a variety of glycolipids like gangliosides. By contrast, the cytoplasmic leaflet is composed mostly of phosphatidylethanolamine (PE), phosphatidylserine (PS) and phosphatidylinositol (PI) and its phosphorylated derivatives (Devaux and Morris, 2004). With regards to sphingolipids and glycerolipids, the asymmetry of the former is established during their biosynthesis and that of the latter requires ATPases such as the amino-phospholipid translocase that transports lipids from the outer to the inner leaflet, as well as Multiple

Drug Resistance proteins that transport PC in the opposite direction (Devaux and Morris, 2004). This ubiquitous scheme encountered in animal cells could apply in plant cells as proposed by (Tjellstrom et al., 2010). Indeed, the authors showed that there is a pronounced transversal lipid asymmetry in root at the PM. Phospholipids and galactolipids dominate the cytosolic leaflet whereas the apoplastic leaflet is enriched in sphingolipids and sterols.

From such a high diversity of the plant PM thus arises the question of the respective contribution of lipids to membrane sub-organization. Our groups recently tackled this aspect by characterizing the order level of liposomes prepared from various plant lipids and labeled with the environment-sensitive probe di-4-ANEPPDHQ (Grosjean et al., 2015). Fluorescence spectroscopy experiments showed that, among phytosterols, campesterol exhibits the strongest ability to order model membranes. In agreement with these data, spatial analysis of membrane organization through multispectral confocal microscopy pointed the strong ability of campesterol to promote Lo domain formation and organize their spatial distribution at the membrane surface. Conjugated sterols also exhibit a striking ability to order membranes. In addition, GIPCs enhance the sterol-induced ordering effect by emphasizing the formation and increasing the size of sterol-dependent ordered domains.

The aim of this study was to re-investigate the lipid composition and organization of the PM with a particular focus on GIPCs using tobacco leaves and BY-2 cell cultures as models. Analyzing all membrane lipid classes at once, including sphingolipids, is challenging because they all display dramatically different chemical polarity going from very apolar (like free sterols) to highly polar molecules (like polyglycosylated GIPCs). Most lipid extraction techniques published thus far use chloroform/methanol mixture and phase partition to remove contaminants, resulting in the loss GIPCs, which remain either in the aqueous phase, unextracted in the insoluble pellet or at the interphase (Markham et al., 2006). In order to gain access to both glycerolipids and sphingolipids species at a glance, we developed a protocol whereby the esterifed or amidified FAs were hydrolyzed from the glycerobackbone (glycerolipids) or the long chain base (sphingolipids) of membrane lipids, respectivley. FA were then analyzed by GC-MS with appropriate internal standards for quantification. We further proposed that the use of Methyl *tert*-

184 butyl ether (MTBE) ensures the extraction of all classes of plant polar lipids. Our results
185 indicate that GIPCs represent up to 40 mol% of total tobacco PM lipids. Interestingly,
186 polyglycolyslated GIPCs are 5-fold enriched in DIMs of BY-2 cell when compared to
187 PM. Further investigation brought us to develop a preparative purification procedure that
188 allowed to obtaining enough material for raising antibodies against GIPCs. Using
189 immunogold-labeling on PM vesicles, it was found that polyglycosylated GIPCs cluster
190 in membrane nanodomains, strengthening the idea that lateral nano-segregation of
191 sphingolipids takes place at the PM in plants. Multispectral confocal microscopy was
192 performed on vesicles prepared using GIPCs, phospholipids and sterols, and labeled with
193 the environment-sensitive probe di-4-ANEPPDHQ. Our results show that, despite a
194 different fatty acid and polar head composition, GIPCs extracted from tobacco leaves and
195 BY-2 cells have a similar intrinsic propensity of enhancing vesicle global order together
196 with sterols. Assuming that GIPCs are mostly present in the outer leaflet of the PM,
197 interactions between sterols and sphingolipids was finally studied by Langmuir
198 monolayer and the area of a single molecule of GIPC, or in interaction with phytosterols,
199 was calculated. Using the calculation docking method, the energy of interaction between
200 GIPCs and phytosterols was determined. A model was proposed in which GIPCs and
201 phytosterols interact together to form Lo domains, and in which the VLCFAs of GIPCs
202 promote interdigitation of the two membrane leaflets. The implication of domain
203 formation and asymmetrical distribution of lipids at the PM in plants is also discussed.
204 Finally, we propose a model that re-considers the intricate organization of the plant PM
205 bilayer.
206

RESULTS

GIPCs are enriched in plasma membrane microdomains

Because FA-containing lipids, i.e. glycerolipids, acylated sterylglucosides and GIPCs, exhibit marked different FA compositions, total FA distribution of microsomal, PM and DIM fractions isolated from BY2 cells and tobacco leaves was determined to test for the assumption that GIPCs mainly reside in PM. Samples were transesterified in hot methanol/sulfuric acid solution to fully release both FA-esterified glycerolipids and sterylglucoside, and FA-amidified sphingolipids. Total FA content was then quantified by GC-MS (see Supplemental Fig. S1, for a typical GC-MS spectrum). The Fig. 1A shows that, in both tobacco leaves and BY-2 cells, the combined percentage of VLCFA and hVLCFA increases from *ca*. 3% in total tissue to *ca*. 55% in DIM at the expense of LCFAs, i.e. 16 and 18 carbon atom-long FA (Fig. 1A; refer to Supplemental Fig. S2 for the detailed FA content). Comparison of FA contents of DIM fractions floating in the sucrose gradient, and Detergent-Soluble Membrane (DSM) fractions in the bottom of the gradient revealed a higher level of LCFAs in DSM, which correlates with a lower percentage of (h)VLCFA in this fraction (Supplemental Fig. S3).

In order to understand the origin of (h)VLCFA, we analyzed the structure of the different family of plant PM lipids. We previously showed that VLCFA and hVLCFA are absent from tobacco glycerolipids, except for a few percent of 20:0/22:0 in PS (Mongrand et al., 2004; Lefebvre et al., 2007). Further extraction and structural analyses revealed that tobacco ASGs consist of saturated FA with mainly 16 and 18 carbon atoms and common sterols of the PM (Supplemental Fig. S4). GluCER that accounts for only 5-10 mol% of PM (Furt et al., 2010) is acylated by h16:0 as major hydroxylated FA (Supplemental Fig. S5). Therefore, we hypothesized that VLCFA and hVLCFA, present in high amount in PM and DIM, likely originate from GIPCs.

To test this hypothesis, we purified total GIPCs from tobacco leaf and BY-2 cells as described in (Bure et al., 2011), and determined their FA and LCB content by GC-MS.

hVLCFA and VLCFA content is highly comparable in DIMs and pure GIPCs (Fig. 1B), with an even higher proportion of hVLCFA in DIMs purified from BY2 cells, suggesting that hVLCFA-containing GIPCs are most likely to be present in membrane microdomains. Besides, levels of the two LCB t18:0 and t18:1, which are mostly present

in GIPCs (Bure et al., 2011), strongly increase in DIMs when compared to PM, reaching 80% of total LCBs in DIMs (Supplemental Fig. S6, and Borner et al., 2005). This is also in good agreement with a strong enrichment of GIPCs in DIMs. Note that h16:0 is enriched in DIMs (Fig. 1B). Logically, this FA is found in tobacco gluCER (Fig. S5), a sphingolipid enriched in tobacco DIMs (Mongrand et al., 2004); (Lefebvre et al., 2007).

To further characterize the enrichment of GIPCs in DIMs, we first compared the total GIPCs extracted from leaf and BY-2 cells by MALDI-TOF mass spectrometry (Bure, et al. 2011). Leaf GIPCs mostly contain GIPCs of series A (with 2 sugars) and BY-2 contain in addition to series A, a vast array of polyglycosylated GIPCs of the B to E series (Fig. 2), as previously described (Bure, et al. 2011). The detailed molecular species of the polar head and LCB/FA combination is provided in Supplemental Fig. S7 with the nomenclature described in (Bure et al., 2011). We next used HP-TLC to separate the different series (Kaul and Lester, 1975) (Fig. 2B), scratched the corresponding silica bands and quantified the FAMES by GC-MS after transmethylation/silylation (Fig. 3 and 4). Note that the series A partitioned into two bands called PhytoSphingoLipid: PSL I (N-Acetyl glucosamine(GlcNAc)-GlcA-IPC) and PSL II (Glucosamine(GlcN)-GlcA-IPC) as previously established (Kaul and Lester, 1975).

GIPC of series A were found in both PM and DIM fractions of tobacco leaves (Supplemental Fig. S8), but the fact that BY-2 cells contain different series of GIPCs prompted us to determine whether polyglycosylated GIPCs were enriched in DIMs of BY-2. We performed HP-TLC coupled to GC-MS, as described above. GIPCs of series B were enriched three times in DIMs when compared to PM, reaching 17% of total GIPCs in BY-2 DIM (Fig. 3).

Lipid composition of tobacco plant PM based on the latter set of data was combined to previous findings (Furt et al., 2010), and the global lipid composition of PM and DIM fractions was recalculated taking into account GIPC concentrations (Fig. 3). As expected, glycerolipids were depleted in DIM fractions when compared to PM, whereas the exact opposite trends was observed for sphingolipids, whether these fractions were prepared from tobacco leaves (Fig. 4A) or BY-2 cells (Fig. 4B). Remarkably, GIPCs that have long been omitted for technical reasons in PM composition, represent up to 45 and 30 mol% of total PM lipids isolated from leaves and BY-2 cell suspensions, respectively.

Furthermore, DIM fractions purified from both BY-2 cells and photosynthetic tissues display a huge proportion of GIPCs that reaches 60 mol%, suggesting that the contribution to sphingolipid enrichment in PM microdomains is mainly due to GIPCs. It is also worth noting that the sum of sterols and sphingolipids averages 90 and 88 mol% in DIM of tobacco leaves (Fig. 3A right) and that of BY-2 cells (Fig. 3B right), respectively. We reasoned that if GIPCs are exclusively located in the outer leaflet of PM (see discussion section), the presence of more than 50 % of GIPCs in DIMs suggests a higher solubilization of the inner leaflet by the TritonX-100.

Hence, from these data arise the question of the lipid-to-protein ratio, commonly thought to be closed to 1 for plant PM. This ratio was experimentally reinvestigated using BY-2 PM samples. One hundred micrograms of PM vesicles were extracted by the "gold-standard" Folch protocol, i.e. chloroform/methanol 2/1 (v/v) extraction. As previously described by (Markham et al., 2006), almost half of the (h)VLCFA-containing GIPCs were lost in the lower aqueous phase (Fig. S9). This phase was therefore evaporated to remove solvents, resuspended in pure water and GIPCs were re-extracted with butanol-1 (which extract 98% of plant GIPC from water as previously shown in Bure et al., 2011). Importantly, no FA was recovered in water after this double extraction (Fig. S9). In addition, when comparing direct transesterification to Folch protocol followed by butanol-1 extraction, the estimated lipid recovery yield using FA levels as proxy was close to 100%, indicating full extraction of lipids irrespectively of their polarity. Based on these results, the lipid-to-protein ratio was calculated to be 1.3 ± 0,07 for BY-2 PM.

We further decided to test other solvents for lipid extraction to get a simple, quantitative and unbiased recovery of lipid species from plants. Methyl *tert*-butyl ether (MTBE) extraction was tested, because it has been shown to allow faster and cleaner lipid recovery (Matyash et al., 2008). Its low density forms the upper layer organic phase during phase separation, which simplifies its recovery (Fig. S10A). We thus compared Folch protocol (Extraction #1 in Experimental section), MTBE extraction (Extraction #2) and Markham protocol (extraction #3) developed to fully extract plant sphingolipids (Markham et al., 2006). Rigorous testing demonstrated that the extraction in hot isopropanol followed by one of the three extractions was suitable to extract total polar

lipids of plant samples (see Experimental section). Nevertheless, Markham's extraction (#3) diplays the disadvantage to contain large amount of water, hardly evaporated, and protein contamination in the organic phase because of the absence of liquid-liquid phase separation. In the Folch extraction (#1), inconvenience resides in the fact that the higher density of chloroform forms the lower phase in the two-phase partitioning system, and a glass pipette or a needle must cross the aqueous phase to collect the lipid-containing one. By contrast, lipid extraction by upper phase MTBE/methanol/water "extraction #2" greatly simplifies sample handling. We therefore proposed the MTBE method as a method of choice to extract total plant polar lipids.

Purification of GIPC series from BY-2 cells and production of antibodies against polyglycosylated GIPCs

Pure GIPCs are not commercially available, neither are the corresponding molecular tools dedicated to their study, like fluorescently-labeled lipids or specific antibodies. We thus purified several milligrams of GIPCs in order to immunize rabbits and raise antibodies to be used in immunolabeling experiments. Because of their anionic phosphate groups, GIPCs can be purified by anion-exchange chromatography on diethylaminoethyl (DEAE) cellulose. This approach has the double advantage of allowing sample cleanup and concentration.

The preparative purification procedure was carried out according to Kaul and Lester (1975) with slight modifications described in the section Material and Methods. Home-packed DEAE cellulose chromatographic column was used for that purpose and GIPCs were eluted with increasing concentrations of ammonium acetate dissolved in chloroform/methanol/water (30/60/8, v/v/v). Under our experimental conditions, GIPCs of series A (namely PSL1 and PSL2) were successfully separated from polyglycosylated GIPC of series B-F; the former eluting in fractions 41-45, whereas the latter eluted in fractions 46-49 (Supplemental Fig. S11A). Glycerolipid contaminations were discarded from these fractions by methylamine treatment, which hydrolyses ester bonds (Markham et al., 2006). Fractions were then dialyzed to remove ammonium acetate and their concentration and purity estimated by GC-MS and MALDI-TOF (Supplemental Fig. S11B). They were subsequently used for preparing liposomes supplemented with

bacterial lipid A known to boost rabbit immunity (Richards et al., 1998). The two immune sera obtained following rabbit injection with GIPC of series A did not react with the DEAE-purified fractions used for the immunization protocol (data not shown). By contrast, one immune serum (rabbit #46) raised against polyglycosylated GIPCs of series B-F clearly reacted with the chromatographic fractions used for the immunization protocol, whereas no reaction was observed with the corresponding pre-immune serum (Figure 5A). ELISA performed on PM showed strong signal increase between negative controls (preimmune serum) and final serum or purified IgG antibodies (Supplemental Fig. S12). No specific signal was detected with antibodies against GIPCs on hydrophobic membranes that have been spotted with all eight phosphoinositides and seven other biological important lipids ("PIP strip", Supplemental Fig. S13). Finally, to further test the specificity of the antibodies on the different GIPCs series purified from BY-2 cells, Eastern blots were directly performed on HP-TLC plates containing PM lipids extracted with the MTBE protocol described above. Rabbit polyclonal antibodies were able to recognize polyglycosylated GIPCs of series B-F, but not those of series A (Fig. 5B).

Polyglycosylated GIPCs cluster within nanodomains in tobacco PM

Since polyglycosylated GIPCs are enriched in BY-2 DIM fractions (Fig. 4B), the possibility of visualizing GIPC-enriched clusters was challenged by transmission electron microscopy using anti-GIPC antibodies-based immunogold labelling experiments. PM vesicles were purified from BY-2 cells, directly deposited onto microscope grids allowing for the exposure of large membrane sheets. The grids were then pretreated to prevent nonspecific binding, incubated first with primary antibodies against polyglycosylated GIPCs and then with secondary IgG conjugated to colloidal gold particles. Preparations were negatively stained with ammonium molybdate to reveal the vesicle morphology and observed by transmission electron microscopy.

Statistical analysis was performed on 49 independent gold-labeled PM vesicles to analyze the putative clustering of gold particles. The mean and standard deviation were calculated for different parameters: diameter of PM vesicles, area of PM vesicle, number of gold per PM vesicle, number of gold particles per cluster, size of gold particle cluster and distance between two neighboring clusters. The mean labeling density was quantified to be 7 gold

particles per vesicle. Groups of particles were composed of an average of 4 gold particles (from 3 to 7 particles were clustered). We calculated that 88% (n=3) of the gold particles showed a clustered distribution throughout the vesicle surface with an average of 4 gold particles, and with an average cluster diameter of 35 nm ± 7nm (Fig. 6A,B). Only 12% of the gold particles exhibited a random distribution on the PM surface. Ripley's K-function analysis indicated that the gold pattern was aggregated, since K(r) values of experimental data laid clearly above the Poisson simulation curve corresponding to completely random pattern (Fig 6C). Negative controls including omission of the primary antibody or use of pre-immune serum exhibited a very weak labeling. Positive controls carried out using antibodies raised against the proton pump ATPase (PMA) showed a heavy labeling of the PM (Raffaele et al., 2009) (Supplemental Fig. S14). Therefore, GIPCs (series B-F) exhibit an aggregated pattern within the PM of BY-2 cells with a mean size of 35nm.

Order level of model membranes prepared with GIPCs isolated from leaves or cell cultures

The ability of GIPCs to change membrane order and organize Lo domain was investigated using the environment-sensitive probe di-4-ANEPPDHQ, as described in (Grosjean et al., 2015). Briefly, membrane organization alters the fluorescence emission spectrum of the probe that emits in both red (635 to 655 nm) and green spectral regions (545 to 565 nm). Increase in green fluorescence emission correlates with a higher average order level of the membrane. Conversely, an emission shift towards red wavelengths indicates a decrease in the relative amount of ordered domains in the lipid bilayer. The Red-to-Green fluorescence ratio of the Membrane (RGM) thus reflects the relative proportions of Ld/Lo phases within membranes (Nichols et al. 1986).

Previously, we showed that plant sphingolipids, especially GIPCs, enhanced the sterol-induced ordering effect by increasing the size of sterol-dependent ordered domains (Grosjean et al., 2015). In order to test for the impact of GIPC's composition on global membrane organization, Large Unilamellar Vesicles (LUV) were prepared using distinct combination of lipids, incubated in the presence of di-4-ANEPPDHQ and the RGM calculated upon spectral acquisition. The phospholipids dioleoylphosphatidylcholine (DOPC) and dipalmitoylphosphatidylcholine (DPPC), the phytosterol (campesterol or a

393 sterol mix isolated from BY2 cells (TM)), and GIPCs were used for producing LUV. We
394 compared GIPCs of series A isolated from tobacco leaves, and GIPCs of series A-F,
395 which include polyglycosylated molecules, purified from BY-2 cell suspensions.
396 Importantly, the ceramide moiety of tobacco leaves mostly contains hVLCFA, whereas
397 that of BY2 suspension harbors an equimolar mix of VLCFA and hVLCFA.
398 Results of Fig. 7 confirmed that GIPCs have no particular ability to modify the order
399 level of model membranes containing only phospholipids and suggest that the size of
400 their sugar head and the hydroxylation of VLCFA do not change this capacity. When
401 33% of campesterol or a sterol mixture mimicking the one found in tobacco BY-2 PM
402 (TM, Tobacco Mix) were added to phospholipids and GIPCs, a significant and similar
403 decrease of the RGM was observed (Fig. 7). Such decrease of RGM confirm the major
404 involvement of sterol in increasing membrane order level, and suggest that 17% of
405 polyglycosylated (Fig. 3) or the presence of 50% of VLCFA (Fig. 1B) in GIPCs does not
406 drastically modify the ability of sphingolipids to order membrane with sterols.
407

408 **Molecular simulation modeling and biophysical analysis reveals GIPC/Sterol**
409 **interaction and interdigitation of GIPC's VLCFA between the two leaflets of the**
410 **PM**

411 Based on the literature (see discussion) and immunolabelling experiments (Fig. 6), we
412 reasonably hypothesized that GIPCs may preferentially reside in the apoplastic leaflet.
413 Therefore, we conducted biophysical experiments and energetic calculation to
414 characterize outer leaflet organization of plant PM, i.e. structure, organization and
415 behavior.
416 The Langmuir trough technique applied on a monolayer model at air–water interface has
417 been extensively used for characterizing interfacial organization of lipids and lipid–lipid
418 interactions at the micrometric level (Deleu, et al. 2014). The GIPC compression
419 isotherm (Fig. 8A) showed a low and relatively constant surface pressure at large
420 molecular areas, corresponding to a gaseous state. Compression of a pure GIPC
421 monolayer induced a progressive increase in surface pressure, indicating the appearance
422 of a liquid-expanded (LE) state, which is characterized by a certain degree of cooperative
423 interaction between the molecules at the interface (Fig. 8A). This was confirmed by the

424 value of the two-dimensional compressibility modulus (Cs^{-1} = 31.9 mN/m in the 180-70
425 Å²/molecule region), which is lower than the highest value (100mN/m) for a LE film
426 (Rideal, 1963). At the onset of the LE state, corresponding to the more expanded
427 configuration, the molecule occupies a mean interfacial area of 209.9±3.6 Å²/molecule.
428 This increase in surface pressure was followed by a small plateau of quite constant
429 surface pressure and by a sharp increase in surface pressure at low areas per molecule.
430 This indicated that GIPC monolayers can adopt a more condensed state (Cs^{-1}>80mN/m)
431 under high compression. In this state, the lipids occupy a mean molecular area of
432 66.0±11.3 Å²/molecule and adopt probably a vertical orientation at the interface.
433 We next assessed the interaction between GIPCs and sitosterol; information can be
434 obtained by a thermodynamic analysis of the compression isotherms of the mixed GIPC-
435 sitosterol monolayers. Within a mixed monolayer, if the two components are immiscible
436 (or ideally miscible), the area occupied by the mixed film will be the sum of the areas of
437 the separate components (obeyed the additivity rule) (Maget-Dana, 1999). Any deviation
438 from the additivity rule can be attributed to specific interaction between the two
439 components (Maget-Dana, 1999; Fang et al., 2003). Whatever the surface pressure
440 considered (10, 20 or 30 mN/m), the mean molecular area of mixed monolayer GIPC/Sito
441 (85/15) was significantly lower than the theoretical value calculated from the additivity
442 rule (Fig. 8B). The negative deviation of the area, together with the negative excess of
443 free energy of mixing (ΔGex) (Fig. 8C) suggests a strong attractive interaction between
444 the two components (Maget-Dana, 1999; Gaines, 1966; Eeman et al., 2005). Moreover,
445 the negative value of ΔGM (Fig. 8C) indicated that the mixed GIPC/sitosterol monolayer
446 is thermodynamically stable.
447 *Molecular modelling of the GIPC monolayer and membrane insertion*
448 We finally used a simple theoretical docking method, called Hypermatrix (HM). This
449 method is particularly useful to compare the specific interaction of a molecule of interest
450 with lipids and with itself, and hence helps to understand its organization according to the
451 different interacting forces. The analysis of the assembly of GIPC molecules with
452 t18:0/h24:0 in a monolayer showed that the calculated interaction is mainly driven by
453 hydrophobic energy (Fig. 9C). The mean interfacial area occupied by one molecule in the
454 monolayer is 69±10 Å² (Fig. 9C). This is in very good agreement with the area measured

455 experimentally using the Langmuir technique in high compression conditions, suggesting
456 that the calculated structure of GIPC corresponds to this configuration. When the
457 interaction between GIPCs and sitosterol was analyzed, the energy of the interaction was
458 comparable to that of GIPC monomolecular layer, with a slight increase in Van der
459 Waals interactions (Fig. 9C). This suggests a good steric fitting between the two
460 molecules, as shown on figure 9A. This molecular fitting can also be correlated to the
461 fact that the mean area calculated in mixed GIPC/sitosterol monolayers was lower than
462 the area of individual molecules (Fig. 9C), again in very good agreement with the
463 experimental assays on monolayer (Fig. 8B).
464 To analyze the behavior of GIPCs with t18:0/h24:0 into a lipid membrane, we calculated
465 its insertion into a simplified implicit bilayer (IMPALA method) (Ducarme et al., 1998)
466 and compared it to gluCER with d18:2/h16:0. Fig. 9B clearly evidenced a significant
467 difference between gluCER and GIPC: 1/ the size of the polar heads and the positioning
468 of acyl chains are strikingly different; 2/ the saturated VLCFA of GIPCs runs out of the
469 middle of the bilayer and interdigitates by at least 6-7 carbon atoms within the second
470 leaflet.
471

DISCUSSION

GIPCs are by far the major lipids of the plant plasma membrane

In this work, we reinvestigated the lipid composition of PM and ordered domain isolated as Detergent-Insoluble Membranes (DIMs), with a particular focus on GIPCs. The latter class of sphingolipids has long been neglected because it is not extracted by conventional lipid extraction procedures (Fig. S9 and Sperling et al., 2005; Markham et al., 2006). Here, we showed that GIPCs represent up to 30-40 mol% of the total PM lipids of tobacco plants and therefore represent the bulk of PM outer leaflet lipids, with 60-80% of total outer leaflet lipids (Fig. 3 and 10). Taking into account this striking result, we recalculated the lipid-to-protein ratio of plant PM and found a ratio of 1.3. Hence, bearing in mind that PM contains a high protein density, it is tempting to propose that plant PM should not be considered as system where proteins are floating in a "sea" of lipids, but as a lipid–protein composite in which a very high density of transmembrane and anchored proteins may modify order on nearby lipids (Jacobson et al., 2007). A recent publication in plants showed for example that PM are subcompartmentalized into a plethora of coexisting and diverse microdomains labeled by the different isoforms of the inner leaflet plant raft protein REMORINs (Jarsch et al., 2014). The respective role of lipids and proteins in this segregation of membrane compounds remains to be elucidated.

GIPC's polar headgroups are much bulkier than phospholipid ones

The volume occupied by the glycosyl-phosphoinositol headgroup of GIPCs increases with the complexity of the oligosaccharide chain. Our experimental data obtained by the Langmuir monolayer technique point that the molecular area occupied by tobacco GIPCs of series A varies from 66.0±11.3 to 209.9±3.6 Å²/molecule from a condensed to an expanded state (Fig. 8A). This was further corroborated by our computational calculations indicating a value of 69±10 Å²/molecule (Fig. 9C) in good agreement with the values of the interfacial area either calculated or measured by Langmuir monolayer technique, as reviewed in (Deleu et al., 2014). By contrast, phospholipids occupy 95-110 Å²/molecule in an expanded state and 45-55 Å²/molecule in a condensed state (Deleu et al., 2001; Eeman et al., 2005) and sterols display an interfacial area of 38-48 Å²/molecule (Eeman et al., 2005; Scheffer et al., 2005). Predictions based on the geometrical

properties of glycosphingolipid molecules indicate that the separation of a glycosphingolipid-rich phase in a phospholipid bilayer would imply a minimization of the interfacial free energy required to accommodate the amphipathic glycosphingolipid in the bilayer. Therefore, the geometrical properties inherent to the bulky headgroup of glycosphingolipids strongly favor phase separation and spontaneous membrane curvature, for review (Sonnino and Prinetti, 2010). In animals, the extent of ganglioside phase separation in glycerophospholipid bilayers depends on the surface area occupied by the oligosaccharide group that is usually directly correlated with the number of sugar residues (Masserini et al., 1989). Nevertheless, one must note that gangliosides are present in very low amount in animal membrane (less than few percent), whereas plant GIPCs represent the major sphingolipids of the PM. In that context, the biophysical properties of the plant PM must be fully reinvestigated.

Role for GIPCs and sterols in coupling the inner and the outer leaflets of the PM

The asymmetry of lipids in the tobacco PM

A common feature of eukaryotic PMs is the non-random distribution of lipids in the two leaflets of the membrane, called lipid asymmetry. Lipid asymmetry within the two PM monolayers is responsible for different biophysical properties and influences numerous cellular functions. The lipid asymmetry lies in the facts that glycerolipids are primarily synthesized on the cytosolic side of cellular membranes whereas production of complex sphingolipids is completed in the ER/Golgi, rendering the latter exposed to the outer surface. In addition, sterols have higher affinity for sphingolipids than glycerolipids. This out-of-equilibrium situation is maintained by the activity of lipid translocases, which compensate for the slow spontaneous transverse diffusion of lipids (Devaux and Morris, 2004).

To build a model of plant PM, we used the results of the present paper, and those obtained by Tjellström and collaborators (2010) who showed that there is a transversal lipid asymmetry in root plant PM. They calculated that the distribution cytosolic/apoplastic leaflet was 65:35 for phospholipids, 30:70 for total sterols, and 30:70 for GluCer. DGDG is exclusively located in the inner leaflet (Tjellstrom et al., 2010). Here, we considered that the glycerophospholipid-rich inner leaflet is unsaturated and

534 that plant phosphatidylserine (PS) and polyphosphoninositides (e.g. PIP_2) were
535 exclusively present in the inner leaflet, as described in animal models (Di Paolo and De
536 Camilli, 2006). As Filipin III labeling used to assess sterol distribution could not
537 discriminate between free sterols and sterol derivatives (ASG and SG) (Tjellstrom et al.,
538 2010), we drew free sterols, SG and ASG equivalently distributed between the two
539 leaflets, with a molar ratio for sterols of 30:70, in:out.
540 We tried to experimentally access the distribution of GIPCs in the PM. We treated Right
541 Side Out (RSO) and In Side Out (ISO) vesicles with Sphingolipid ceramide N-deacylase
542 (SCD) enzyme able to hydrolyze GIPCs (Blaas and Humpf, 2013), as described with
543 phospholipase A2 for phospholipid asymmetrical distribution (Tjellstrom et al., 2010). In
544 our hands, no GIPC hydrolysis occurred (data not shown). Nevertheless, we reasonably
545 hypothesized that GIPCs are exclusively located in the apoplastic face for different
546 independent reasons: 1/ the two first steps of the GIPC synthesis (IPC synthase and
547 glucuronic transferase) occur in the Golgi apparatus (Wang et al., 2008); (Rennie et al.,
548 2014); 2/ The mannosylation of series A of GIPC to build series B is dependent of the
549 GDP-mannose transporter GOLGI-LOCALIZED NUCLEOTIDE SUGAR
550 TRANSPORTER (GONST1), suggesting a luminal glycosylation of GIPCs so that the
551 polar heads is exposed in the outer leaflet of the PM after vesicular fusion (Mortimer et
552 al., 2013); 3/ GIPCs are structurally homologs to gangliosides, exclusively present in the
553 outer leaflet of the PM in animal cells (Sonnino and Prinetti, 2010); 4/ it is very unlikely
554 that GIPCs may spontaneously flip-flop in the PM because of the size and polarity of
555 their heads and 5/ immunogold labeling of GIPCs (series B-F) on PM vesicles seems to
556 be unilaterally distributed mainly outside of the PM vesicles (Fig. 6).

557 ***Saturated very long chain fatty acid of GIPCs interdigitate the two leaflets***

558 A key question in understanding the functional role of the PM is whether lipids of the
559 outer leaflet are coupled to those of the inner leaflet. Plant GIPCs exhibit a high content
560 of VLCFA that can be hydroxylated on carbon 2. The presence of VLCFA in DIMs was
561 recently observed in bean and maize DIMs (Carmona-Salazar et al., 2015). Here, the
562 modeling approach suggests a strong and stable interdigitation of (h)VLCFA of GIPCs
563 from the outer leaflet into the inner leaflet by 6-7 carbon atoms (Fig. 9B). VLCFA are
564 also abundant in sphingolipids in animal cells. It has been proposed that lipid bilayer

565 organization of the *stratum corneum* could be stabilized by a partial interdigitation
566 between the two leaflets (Ruettinger et al., 2008). Interdigitation of long chain fatty acid
567 residues between complex lipids might thus represents a common feature in plants and
568 animals that allows a higher thermal stability of the outer leaflet, as described in artificial
569 asymmetrical liposomes prepared with animal lipids (Cheng et al., 2009).
570
571 **GIPCs are able to organize in liquid-ordered domains with sterols**
572 Tobacco cells produce several hundred GIPCs of different structures, (see Fig. 2, and
573 Cacas et al., 2013), with the same ceramide moiety and a variable glycan part.
574 Publication of the 70's suggest that up to 20 sugars can be added to the GIPC core
575 structure, but little is known about such molecule (Kaul and Lester, 1975). In this paper,
576 we demonstrated that GIPCs with more than two sugars are enriched in DIMs (Fig 2C)
577 and these complex sphingolipids cluster in domains of 35 nm (Fig. 6). In addition, we
578 showed that 2-hydroxylated-containing GIPCs were enriched in DIMs (Fig. 1B). This
579 result is coherent with biophysical studies where raft phase separation is favored by the
580 fact that sphingolipids, as ceramide-based amphipathic lipids, can create a network of
581 hydrogen bonds due to the presence of the amide nitrogen, the carbonyl oxygen and the
582 hydroxyl group positioned in proximity of the water/ lipid interface of the bilayer
583 (Pascher, 1976). In addition, GIPC's LCB being dominated by tri-hydroxylated LCBs
584 (Figs S6), the presence of two additional hydroxyl groups at the interface may be of
585 importance for sphingolipid/phytosterol interactions. The contribution of hydrogen bonds
586 between lipids stabilizing a more rigid segregated phase in the bilayer is energetically
587 remarkable (Quinn and Wolf, 2009). We recently showed that GIPCs enhance the sterol-
588 induced ordering effect by stimulating the formation of and increasing the size of sterol-
589 dependent ordered membrane domains (Grosjean et al., 2015), suggesting a strong
590 interaction between phytosterols and GIPCs leading to a well defined Lo phase
591 separation. Docking calculation between phytosterols and GIPCs showed that the
592 interaction is mostly of hydrophobic and Van der Waals types (Fig. 9C). Hence, the closer
593 the molecules are, the stronger the interaction is. This aspect is also pointed by Langmuir
594 monolayers' experiments, where we measured an attractive interaction between GIPCs
595 and phytosterols at a molar ratio of 85:15 (Fig. 8). Finally, interdigitated hydrocarbon

chains may play a role in the stabilization of lipid domains, as reviewed in (Sonnino and Prinetti, 2010).

A model summarizing these data is presented in the figure 10. To build this model, the molar composition of lipids from BY-2 PM (Fig. 4) and information presented above were considered. This model emphasizes the strong enrichment of GIPCs in the apoplastic phase of the PM. In accordance with this assumption, only little space would be left in the outer leaflet for phospholipids, which consequently are concentrated on the cytoplasmic leaflet. Polyglycosylated GIPCs cluster with sterols in domains of ca. 35nm in the outer leaflet, and polyphosphoinositide-enriched domain are present in the inner leaflet according to our previous work (Furt et al., 2010).

Are rafts in the two leaflets coupled?

Plant GIPCs are clearly involved in raft formation, and rafts exist in both external and internal leaflets of the plant PM (Raffaele et al., 2009); (Furt et al., 2010); (Mongrand et al., 2010). "Biological rafts" are likely of nanometer scale and certainly differ in size and stability in the two monolayers. It is not known whether they overlap so that they are coupled functionally and structurally (Eisenberg et al., 2006); (Subczynski and Kusumi, 2003). By exploring this possibility, one could shed light on how cues are transmitted through the bilayer. Does the clustering of proteins or lipids in the outer leaflet trigger the re-arrangement of downstream proteins or lipids in the inner leaflet (Kinases, phosphatases, small G proteins, PIP_2…), leading to signal transduction and amplification? Can rafts in the outer leaflet enriched in GIPCs and sterols mirrored by PIP_2-enriched cytoplasmic leaflet rafts, as represented in figure 10? What could be the role of FA interdigitation and lipid asymmetry in plants, and how is this process regulated? Proteins -omitted in our model- will certainly influence raft composition, size, shape and overall physical properties, independently of thermodynamic considerations of the pure lipid phases (Devaux and Morris, 2004). This last aspect remains to be fully elucidated in plant PM.

CONCLUSIONS

In plants, GIPCs have been shown to be involved in early stages of symbiosis (Hernandez et al., 1995), in Golgi and ER integrity (Chen et al., 2008), growth and hypersensitive response through salicylic acid production (Mortimer et al., 2013). A recent study on cell wall rhamnogalacturonan II (RG-II) showed that GIPCs are able to bind RG-II, possibly *via* a Boron bridge, and that they can favor the Boron-dependent dimerisation of RG-II (Voxeur and Fry, 2014). Cell wall is an important feature in regulating protein lateral mobility. In plant cells, turgor pressure tightly pressed PM against cell wall. Martinière and collaborators, 2012 showed that this intimate connection affects protein lateral mobility including the one in the inner leaflet. This suggests that the plant cell wall, and by extension the continuum between the PM and the cell wall, influences protein lateral mobility (Martiniere et al., 2012). This regulation of protein lateral mobility by the cell wall certainly plays a role in plant cellular processes. GIPCs may also be important determinants in cell signaling, cell-to-cell communication, plant defense and the sorting of proteins, as it is also described for complex sphingolipids in animal development (Worrall et al., 2003). The link between outer leaflet lipids and the cell wall also deserves to be fully investigated. Finally, apoplastic leaflet that contains high ordered-forming lipids (GIPC/phytosterols) likely represents physical barrier involved in maintenance of thermal tolerance (Cheng et al., 2009), cell integrity and responses to pathogens. Preparation of asymmetric vesicles that mimic the plant PM will be of great interest to study this coupling, the effect of lipid raft formation and the distribution of transmembrane protein helices (Cheng et al., 2009). In animals, alteration of lipid asymmetry plays a prominent role during cell fusion, activation of the coagulation cascade and, recognition and removal of apoptotic cell. Our work should pave the way to address such questions in plants.

MATERIAL and METHODS

Materials—High-performance thin-layer chromatography (HP-TLC) plates were Silicagel 60 F254 (Merck, Rahway, NJ).

Plant Materials—Leaves were obtained from 8-week-old tobacco plants (*Nicotiana tabacum* cv. Xanthi) grown in a growth chamber at 25°C under 16/8-h day/night conditions. Wild type BY-2 cells (*Nicotiana. tabacum* cv. Bright Yellow 2) and *Vitis vinifera L.* cv 'Cabernet Sauvignon' (CS6) were grown as previously described in (Morel et al., 2006) and (Cacas et al., 2013).

Preparation and Purity of Tobacco PM—All steps were performed at 4°C. PMs were obtained after cell fractionation according to (Mongrand et al., 2004) by partitioning in an aqueous polymer two-phase system with polyethylene glycol /dextran.

Fatty acids Analysis— Each sample was transmethylated at 110°C overnight in methanol containing 5% (v/v) sulfuric acid and spiked with 10 µg of heptadecanoic acid (c17:0) and 10 µg of 2-hydroxy-tetradecanoic acid (h14:0) as internal standards. After cooling, 3 mL of NaCl (2.5%, w/v) were added, and the released fatty acyl chains were extracted in hexane. Extracts were washed with 3 mL of saline solution (200 mM NaCl, 200 mM Tris, pH 8.0), dried under a gentle stream of nitrogen, and dissolved in 150 µL of BSTFA (N,O-bis(trimethylsilyl) trifluoroacetamide) and TMCS (trimethylchlorosilane). Free hydroxyl groups were derivatized at 110°C for 30 min, surplus BSTFA-TMCS was evaporated under nitrogen, and samples were dissolved in hexane for analysis using GC-MS under the same conditions as described in (Bure et al., 2011). Quantification of fatty acids and hydroxyl acids was based on peak areas, which were derived from Total Ion Current (Rehman et al.), and using the respective internal standards.

Sphingoid Base (LCB) Analysis—Samples were heated at 110C for 24 h with 4 mL of dioxane (Sigma) plus 3.5 mL of 10% (w/v) aqueous Ba(OH)2 (Sigma). The sphingoid bases were oxidized to their corresponding aldehydes by stirring the sample with 100 µL

682 of 0.2 M sodium periodate (Sigma) at room temperature for 1 h in the dark. The
683 aldehydes were recovered by hexane extraction and used directly for GC analysis as
684 described in (Cacas et al., 2012a).
685
686 **Extraction of total polar lipids; Set up of lipid extraction protocol for total polar**
687 **lipids in plants**—Membrane fractions (100-200µg) or grape cell culture (*ca*. 20 mg of
688 lyophilized materiel) were extracted according to three independent methods: ***Extraction***
689 ***#1:*** 3.5 mL of chloroform/methanol/HCl (200/100/1, v/v/v) supplemented with 0.01%
690 butylatedhydroxytoluene (BHT) (w/v) were incubated with the sample. Then, 2mL of
691 NaCl 0.9% (w/v) were added, vortexed for 5 min and centrifuged. The lower organic
692 phase was collected, and the higher phase was re-extracted once with 4 mL of pure
693 chloroform. ***Extraction #2:*** 3.5 mL of Methyl *tert*-butyl ether (MTBE)/methanol/water
694 (100/30/25, v/v/v) supplemented with 0,01% BHT (w/v) were incubated with the sample.
695 Then, 2ml of NaCl 0.9% was added, vortexed for 5 min and centrifuged. The upper
696 organic phase was collected, and the lower phase was re-extracted once with 4 mL of
697 pure MTBE. In both extractions, the organic phases were combined and dried. The
698 aqueous phases were dried to remove any trace of organic solvent, resuspended in 1mL
699 of pure water, and GIPCs were back-extracted twice by 1 mL butanol-1. ***Extraction #3***
700 adapted from (Markham et al., 2006): 3.5 mL of (lower phase of propan-2-
701 ol/hexane/water, 55:20:25 (v/v/ v)) were incubated with the sample. The sample was
702 incubated at 60 °C for 15 min with occasional shaking. The extract was spun at 500 g
703 while still warm, and the supernatant was transferred to a fresh tube. The pellet was
704 extracted once more, each time with 3.5 mL of extraction solvent, and the supernatants
705 were combined and dried. The pellet was dried to remove any trace of organic solvent,
706 resuspended in 1mL of pure water, and GIPC were back-extracted twice by 1mL butanol-
707 1. Extracted lipids were dissolved in chloroform /methanol/water (30/60/8, v/v/v) for
708 storage. Alternatively, before lipid extraction, biological samples were transferred to
709 isopropanol (3mL) with 0.01% BHT at 75 °C and incubated for 15 min to inhibit lipase
710 activity.
711 The rationale for the three lipid extraction protocols is presented in Fig. S10A in
712 supplemental data. We used lyophilized grape cell culture (*Vitis vinifera)*, previously

shown to contain similar (h)VLFCA and GIPCs as tobacco cells (Cacas et al., 2013), see Supplemental Fig. S10B. We first compared Folch protocol (Extraction #1) and MTBE extraction (Extraction #2) followed by butanol-1 extraction of the aqueous phase, with Markahm protocol (Extraction #3) shown to fully extract plant sphingolipids (Fig. 4B) (Markham et al., 2006). Results of Fig. S10C *middle* showed that all the classes of lipids were extracted with no significant differences between the three different protocols. We performed a HP-TLC plate to test the integrity of polar lipids, and we observed, as often described during plant lipid extraction, a major activation of Phospholipase D leading to the conversion of phospholipids into Phosphatidic Acid, PA (Supplemental Fig. S10D). To circumvent this problem, we boiled the lyophilized grape cells in hot isopropanol, and further extracted with the three protocols. To our surprise, all the polar lipids including VLCFA-containing GIPCs were extracted without the need of the second extraction step by butanol-1 of the aqueous phase (Fig. S10C *right*). As expected, no degradation of phospholipids was anymore observed on TLC plates (see Supplemental Fig. S10D).

Extraction and purification of GIPCs by DEAE chromatography —GIPCs were purified according to (Bure et al., 2011) and (Grosjean et al., 2015) to obtain milligram amount. Alternatively, GIPCs were purified DEAE chromatography. DEAE Sephadex DE-52 (Whatman pre-swollem, µgranular) was suspended in chloroform/ methanol/water (30:60:8, v/v/v) supplemented with 1M ammonium acetate. A glass column (40 cm high, 2.2 cm of diameter) was plugged by defatted cotton, filled with DEAE Sephadex and washed with 600 mL of chloroform/ methanol/water (30:60:8, v/v/v). GIPC whitish pellet extracted from BY-2 cell culture was dissolved in 10 ml of chloroform/methanol/water (30:60:8, v/v/v) and loaded on the column. The column was washed with 800 ml of chloroform/ methanol/water (30:60:8, v/v/v) for removal of neutral compounds: fractions 1-8. The fractions were sequentially eluted with 500 mL of chloroform/ methanol/water (30:60:8, v/v/v) supplemented with 5 mM ammonium acetate: fractions 9-14, 10 mM ammonium acetate: fractions 15-20; 25 mM ammonium acetate: fractions 21-28; 50 mM ammonium acetate: fractions 29-35; 100 mM ammonium acetate: fractions 36-43; 250 mM ammonium acetate: fractions 44-49, see Fig. S11 in supplemental information. The purification process was monitored by on HP-TLC impregnated with freshly prepared 0.2

744 M ammonium acetate dissolved in methanol, and chromatographed in chloroform/
745 methanol/ NH_4OH (4N in water) (9:7:2, v/v). Lipids were visualized by spraying plates
746 with primuline. GIPC-containing fractions were dissolved in water, and dialyzed against
747 water at 4 °C for two days to remove ammonium acetate (Spectra/Por Dialysis
748 Membrane, MWCO 3500). The water was changed every 6h. The desalted fractions were
749 dried and dissolved in a volume of 3 mL of chloroform/methanol/water (30:60:8, v/v/v),
750 and stored at 4°C.
751
752 **Generation of rabbit polyclonal antibodies to GIPC**—*Preparation of liposomes:*
753 Liposomes were prepared essentially as described previously (Richards et al., 1998).
754 Liposomes for the primary immunization were composed of purified BY-2 cell GIPCs
755 (series A or mix of series B-E), phosphatidylcholine, phosphatidylglycerol, cholesterol in
756 mole ratios of 0.9 / 0.1 / 0.75. Lipid A was included in the liposomes at 20 nmol of lipid
757 A per µmol of phospholipid. Lipids were dried from chloroform/Methanol/water 30/60/8
758 solution. The liposomes were swollen in 1 mL of TBS by vigorous shaking in a vortex
759 mixer, and sonicated at room temperature for 30 min. *Immunization of rabbits*: Rabbits
760 were immunized four times at 0, 21, 42 days (COVALAB - France Biotechnologies,
761 France). Preimmune serum compare with 53 days post injection serum were analyzed.
762
763 **Immunogold labeling of purified plant plasma membranes**— Labeling was performed
764 on purified BY-2 cell PM vesicles according to (Noirot et al., 2014). Immunological
765 reaction on grids was performed for 1h with rabbit polyclonal antibody against
766 polyglycosylated GIPCs (46) diluted 1/40 which was revealed with a goat anti-rabbit IgG
767 conjugate (Aurion, Wageningen, The Netherlands) labeled to 6-nm colloidal gold
768 particles. Three independent experiments using three independent biochemical PM
769 purifications from BY-2 cells were recorded. For each experiment, 3 replicates of
770 immunolabeling and 2 replicates of each control sample (omission of the primary
771 antibody and use of the preimmune) were observed with a Hitachi H7500 transmission
772 electron microscope equipped with an AMT camera driven by AMT software. In order to
773 characterize the distribution of the detected antigen on PM vesicle surface, the density of
774 labeling was evaluated by counting the number of colloidal gold particles per labeled

vesicle. Groups of gold labeling were visualized and size(s) of the cluster(s) were measured on each labeled vesicle with the AMT software. Proportions of gold particles in groups and of isolated gold particles were evaluated. Counting and measurement were performed on 49 pictures of PM vesicles from the three independent experiments. The spatial distribution was determined as described in (Noirot et al., 2014) using the Ripley function (Ripley, 1976).

Order Level Measurement of Artificial Membranes—Preparation of LUVs and Fluorescence spectroscopy, membrane order level Measurement were as described in (Grosjean et al., 2015)

Home made Lipid-blot— Immun-Blot PVDF Membrane (Bio-rad) were activated with methanol for 30 sec. GIPC DEAE fractions (3µl) were deposited and let dried. Membranes were further re-activated in methanol for 2 sec, blocked in TBS supplemented with 5% de-fatted BSA for 1 h. Antibodies to GIPC (dilution 1/100) were incubated for 1h at room temperature, membranes were then rinsed three times with TBS supplemented with 0.1% (v/v) Tween 20, and revealed with anti-rabbit secondary antibodies coupled to horse-radish peroxidase (1/100).

ELISA— All steps were performed at 37°C. ELISA plate were filled with or without 500ng of BY-2 cell PM vesicles in 0,1mL PBS for 2h, then blocked for 2h with 1% BSA in PBS. Anti-GIPC antibodies (dilution 1/50 for sera or 1/100 for purified IgG) were incubated for 1h and revealed with anti-rabbit secondary antibodies coupled to alkaline phosphatase (1/5000). Reaction with p-Nitrophenyl Phosphate (0,01% in 10% diethanolamine buffer) was read at 405 nm after 1h.

Langmuir trough—Total BY-2 GIPC (molecular weight, *ca*. 1260 g/mol) was used in this study. A solution at 0.39mM in chloroform/methanol/water (30/60/8) was prepared. Sitosterol was purchased from Avanti Polar Lipids (Alabaster, USA). It was dissolved at 0.39 mM in chloroform/methanol (2/1). The Π-A isotherms were recorded by means of an automated Langmuir trough (KSV Minitrough, width: 75 mm, area: 24.225 mm², KSV

Instruments, Helsinki, Finland) equipped with a platinum plate attached to a Wilhelmy type balance. The GIPC sample was heat up at 60°C for 15 minutes for a better solubilization. Pure solutions and (0.15/0.85) molar mixtures of Sitosterol/GIPC were spread (fixed volume of 30µL) as tiny droplets to produce a uniform monolayer on a Tris/NaCl 10/150 mM (Millipore Co., Milford, MA) subphase adjusted at pH 7 with HCl. After evaporation of the solvent (15 min), monolayers were compressed at a rate of 5 mm/min and at a temperature of 22 ± 1° °C. Before each experiment, the cleanliness of the system was confirmed by checking the surface pressure over the surface compression of the pure subphase. The reproducibility of the Π-A isotherms was checked by repeated recordings and the relative standard deviation in surface pressure and area was found to be ≤3%.

Molecular modeling approaches—The conformation of GIPC sitosterol and glucosylceramide (d18:2(delta4, delta8)/h16:0) was calculated using the structure tree procedure, as described elsewhere (Lins et al., 1996). The Hypermatrix (HM) docking procedure was used to study the monolayer formed by GIPC and its interaction with sitosterol, as already described (Lins et al., 1999) (Fa et al., 2007) (Bensikaddour et al., 2008) and reviewed recently, (Deleu et al., 2014). Briefly, one GIPC molecule is positioned and fixed for the whole calculation at the center of the system, oriented at the hydrophobic (Haimi et al.)/hydrophilic (phi) interface (Brasseur, 1990). The interacting GIPC (for GIPC monolayer) or sitosterol (for mixed monolayer) is also oriented at the pho/phi interface and, by rotations and translations, more than 10^7 positions of the interacting molecule around the central molecule are calculated. The energy values together with the coordinates of all assemblies are stored in a matrix and classified according to decreasing values. The most stable matching is used to decide the position of the first interacting molecule. The position of the second one is then defined as the next most energetically favorable orientation stored in the matrix taking steric and energetic constraints due to the presence of the first molecule into account. The process ends when the central molecule is completely surrounded with the other molecule. In this method, the lipid/water interface was taken into account by linearly varying the dielectric constant ε between 3 (above the interface) and 30 (below the interface) and an empirical

837 equation for the hydrophobic energy is added in the force field, as described in (Lins and
838 Brasseur, 1995). The mean area occupied by one molecule in the complex was estimated
839 by projection on the x-y plane using a grid of 1 Å square.
840 To calculate the insertion of GIPCs or Soy bean glucosylceramide into an implicit
841 simplified bilayer, we used the IMPALA method described previously (Ducarme et al.,
842 1998). Briefly, this method simulates the insertion of any molecule into a bilayer by
843 adding energy restraint functions to the usual energy description of molecules. The lipid
844 bilayer is defined by C(z), which represents an empirical function describing membrane
845 properties. This function is constant in the membrane plane (x- and y- axes) but varies
846 along the bilayer thickness (z-axis). Two restraints simulate the membrane, one the
847 bilayer hydrophobicity (Epho), and the other, the lipid perturbation (Elip). All the
848 equations were described elsewhere (Ducarme et al., 1998). The method was notably
849 successfully applied to small helical peptides of known configurations (Lins et al., 2001).
850 It provides insights of the behavior of peptide dynamics that cannot be obtained with
851 statistical approaches. All calculations were performed on a Linux station bi-xeon quad
852 core, using the home-designed Z-ultime software.
853

ACKNOWLEDGEMENTS

We thank Yohann Boutté and Patrick Moreau (LBM, Bordeaux) for critical reading of the manuscript. We thank Michel Laguerre (IECB, Bordeaux) for the modelisation of series A tobacco GIPC, Elodie Noirot (PF DimaCell, UMR Agroécologie, Dijon) and Kiên Kiêu (INRA, UR341 Mathématiques et Informatique Appliquées, Jouy-en-Josas) for spatial statistical analysis. We also acknowledge Paul Gouguet (LBM, Bordeaux) Bernadette Codeville (Unité de Glycobiologie, Villeneuve d'Ascq) for the help in GIPC purification, Veronique Aubert for her help in microscopy studies (PF DimaCell, UMR Agroécologie), and Michel Ponchet (Institut Sophia Agrobiotech) for providing tobacco leaves, and Yann Guérardel for the purification material (Unité de Glycobiologie, Villeneuve d'Ascq).

LITERATURE CITED

Bensikaddour, H., Fa, N., Burton, I., Deleu, M., Lins, L., Schanck, A., Brasseur, R., Dufrene, Y.F., Goormaghtigh, E., and Mingeot-Leclercq, M.P. (2008). Characterization of the interactions between fluoroquinolone antibiotics and lipids: a multitechnique approach. Biophysical journal **94,** 3035-3046.

Blaas, N., and Humpf, H.U. (2013). Structural profiling and quantitation of glycosyl inositol phosphoceramides in plants with Fourier transform mass spectrometry. Journal of agricultural and food chemistry **61,** 4257-4269.

Borner, G.H., Sherrier, D.J., Weimar, T., Michaelson, L.V., Hawkins, N.D., Macaskill, A., Napier, J.A., Beale, M.H., Lilley, K.S., and Dupree, P. (2005). Analysis of detergent-resistant membranes in Arabidopsis. Evidence for plasma membrane lipid rafts. Plant physiology **137,** 104-116.

Brasseur, R. (1990). TAMMO: theoretical analysis of membrane molecular organisation,. In Mol. Descr. Biol. Membr. Components by Comput. Conform. Anal., (CRC Press, Boca Raton), pp. pp. 203–219.

Bure, C., Cacas, J.L., Wang, F., Gaudin, K., Domergue, F., Mongrand, S., and Schmitter, J.M. (2011). Fast screening of highly glycosylated plant sphingolipids by tandem mass spectrometry. Rapid communications in mass spectrometry : RCM **25,** 3131-3145.

Cacas, J.L., Melser, S., Domergue, F., Joubes, J., Bourdenx, B., Schmitter, J.M., and Mongrand, S. (2012a). Rapid nanoscale quantitative analysis of plant sphingolipid long-chain bases by GC-MS. Analytical and bioanalytical chemistry **403,** 2745-2755.

Cacas, J.L., Bure, C., Furt, F., Maalouf, J.P., Badoc, A., Cluzet, S., Schmitter, J.M., Antajan, E., and Mongrand, S. (2013). Biochemical survey of the polar head of plant glycosylinositolphosphoceramides unravels broad diversity. Phytochemistry **96,** 191-200.

Cacas, J.L., Furt, F., Le Guedard, M., Schmitter, J.M., Bure, C., Gerbeau-Pissot, P., Moreau, P., Bessoule, J.J., Simon-Plas, F., and Mongrand, S. (2012b). Lipids of plant membrane rafts. Progress in lipid research **51,** 272-299.

Carmona-Salazar, L., El Hafidi, M., Gutierrez-Najera, N., Noyola-Martinez, L., Gonzalez-Solis, A., and Gavilanes-Ruiz, M. (2015). Fatty acid profiles from the plasma membrane and detergent resistant membranes of two plant species. Phytochemistry **109,** 25-35.

Carter, H.E., Gigg, R.H., Law, J.H., Nakayama, T., and Weber, E. (1958). Biochemistry of the sphingolipides. XI. Structure of phytoglycolipide. The Journal of biological chemistry **233,** 1309-1314.

Cheng, H.T., Megha, and London, E. (2009). Preparation and properties of asymmetric vesicles that mimic cell membranes: effect upon lipid raft formation and transmembrane helix orientation. The Journal of biological chemistry **284,** 6079-6092.

Deleu, M., Crowet, J.M., Nasir, M.N., and Lins, L. (2014). Complementary biophysical tools to investigate lipid specificity in the interaction between bioactive molecules and the plasma membrane: A review. Biochimica et biophysica acta **1838,** 3171-3190.

Deleu, M., Nott, K., Brasseur, R., Jacques, P., Thonart, P., and Dufrene, Y.F. (2001). Imaging mixed lipid monolayers by dynamic atomic force microscopy. Biochimica et biophysica acta **1513,** 55-62.

Devaux, P.F., and Morris, R. (2004). Transmembrane asymmetry and lateral domains in biological membranes. Traffic **5,** 241-246.

Di Paolo, G., and De Camilli, P. (2006). Phosphoinositides in cell regulation and membrane dynamics. Nature **443,** 651-657.

Ducarme, P., Rahman, M., and Brasseur, R. (1998). IMPALA: a simple restraint field to simulate the biological membrane in molecular structure studies. Proteins **30,** 357-371.

Eeman, M., Deleu, M., Paquot, M., Thonart, P., and Dufrene, Y.F. (2005). Nanoscale properties of mixed fengycin/ceramide monolayers explored using atomic force microscopy. Langmuir : the ACS journal of surfaces and colloids **21,** 2505-2511.

Eisenberg, S., Shvartsman, D.E., Ehrlich, M., and Henis, Y.I. (2006). Clustering of raft-associated proteins in the external membrane leaflet modulates internal leaflet H-ras diffusion and signaling. Molecular and cellular biology **26,** 7190-7200.

Fa, N., Lins, L., Courtoy, P.J., Dufrene, Y., Van Der Smissen, P., Brasseur, R., Tyteca, D., and Mingeot-Leclercq, M.P. (2007). Decrease of elastic moduli of DOPC bilayers induced by a macrolide antibiotic, azithromycin. Biochimica et biophysica acta **1768,** 1830-1838.

Fang, K., Zou, G., and He, P. (2003). Dynamic viscoelastic properties of spread monostearin monolayer in the presence of glycine. Journal of colloid and interface science **266,** 407-414.

Frazier, Z., and Alber, F. (2012). A computational approach to increase time scales in Brownian dynamics-based reaction-diffusion modeling. Journal of computational biology : a journal of computational molecular cell biology **19,** 606-618.

Furt, F., Simon-Plas, F., and Mongrand, S. (2011). Lipids of the plasma membrane. In The Plant Plasma Membrane. Plant Cell Monographs 19., A.S. Murphy, P. Wendy, and B. Schulz, eds (Heidelberg: Springer-Verlag), pp. 3-30.

Furt, F., Konig, S., Bessoule, J.J., Sargueil, F., Zallot, R., Stanislas, T., Noirot, E., Lherminier, J., Simon-Plas, F., Heilmann, I., and Mongrand, S. (2010). Polyphosphoinositides are enriched in plant membrane rafts and form microdomains in the plasma membrane. Plant physiology **152,** 2173-2187.

Gaines, G.L. (1966). Insoluble Monolayers at liquid-gas Interfaces (

Garssen, M.P., van Koningsveld, R., van Doorn, P.A., Merkies, I.S., Scheltens-de Boer, M., van Leusden, J.A., van Schaik, I.N., Linssen, W.H., Visscher, F., Boon, A.M., Faber, C.G., Meulstee, J., Prick, M.J., van den Berg, L.H., Franssen, H., Hiel, J.A., van den Bergh, P.Y., and Sindic, C.J. (2007). Treatment of Guillain-Barre syndrome with mycophenolate mofetil: a pilot study. Journal of neurology, neurosurgery, and psychiatry **78,** 1012-1013.

Grosjean, K., Mongrand, S., Beney, L., Simon-Plas, F., and Gerbeau-Pissot, P. (2015). Differential effect of plant lipids on membrane organization: hot features and specificities of phytosphingolipids and phytosterols. The Journal of biological chemistry.

Haimi, P., Uphoff, A., Hermansson, M., and Somerharju, P. (2006). Software tools for analysis of mass spectrometric lipidome data. Anal Chem **78,** 8324-8331.

Hernandez, L.E., Perotto, S., Brewin, N.J., and Drobak, B.K. (1995). A novel inositol-lipid in plant-bacteria symbiosis. Biochemical Society transactions **23,** 582S.

Jacobson, K., Mouritsen, O.G., and Anderson, R.G. (2007). Lipid rafts: at a crossroad between cell biology and physics. Nature cell biology **9,** 7-14.

Jarsch, I.K., Konrad, S.S., Stratil, T.F., Urbanus, S.L., Szymanski, W., Braun, P., Braun, K.H., and Ott, T. (2014). Plasma Membranes Are Subcompartmentalized into a Plethora of Coexisting and Diverse Microdomains in Arabidopsis and Nicotiana benthamiana. The Plant cell **26,** 1698-1711.

Kaul, K., and Lester, R.L. (1975). Characterization of Inositol-containing Phosphosphingolipids from Tobacco Leaves: Isolation and Identification of Two Novel, Major Lipids: N-Acetylglucosamidoglucuronidoinositol Phosphorylceramide and Glucosamidoglucuronidoinositol Phosphorylceramide. Plant physiology **55,** 120-129.

Lefebvre, B., Furt, F., Hartmann, M.A., Michaelson, L.V., Carde, J.P., Sargueil-Boiron, F., Rossignol, M., Napier, J.A., Cullimore, J., Bessoule, J.J., and Mongrand, S. (2007). Characterization of lipid rafts from Medicago truncatula root plasma membranes: a proteomic study reveals the presence of a raft-associated redox system. Plant physiology **144,** 402-418.

Lins, L., and Brasseur, R. (1995). The hydrophobic effect in protein folding. FASEB journal : official publication of the Federation of American Societies for Experimental Biology **9,** 535-540.

Lins, L., Charloteaux, B., Thomas, A., and Brasseur, R. (2001). Computational study of lipid-destabilizing protein fragments: towards a comprehensive view of tilted peptides. Proteins **44,** 435-447.

Lins, L., Brasseur, R., Malaisse, W.J., Biesemans, M., Verheyden, P., and Willem, R. (1996). Importance of the hydrophobic energy: structural determination of a hypoglycemic drug of the meglitinide family by nuclear magnetic resonance and molecular modeling. Biochemical pharmacology **52,** 1155-1168.

Lins, L., Thomas-Soumarmon, A., Pillot, T., Vandekerchkhove, J., Rosseneu, M., and Brasseur, R. (1999). Molecular determinants of the interaction between the C-terminal domain of Alzheimer's beta-amyloid peptide and apolipoprotein E alpha-helices. Journal of neurochemistry **73,** 758-769.

Maget-Dana, R. (1999). The monolayer technique: a potent tool for studying the interfacial properties of antimicrobial and membrane-lytic peptides and their interactions with lipid membranes. Biochimica et biophysica acta **1462,** 109-140.

Markham, J.E., Li, J., Cahoon, E.B., and Jaworski, J.G. (2006). Separation and identification of major plant sphingolipid classes from leaves. The Journal of biological chemistry **281,** 22684-22694.

Martiniere, A., Lavagi, I., Nageswaran, G., Rolfe, D.J., Maneta-Peyret, L., Luu, D.T., Botchway, S.W., Webb, S.E., Mongrand, S., Maurel, C., Martin-Fernandez, M.L., Kleine-Vehn, J., Friml, J., Moreau, P., and Runions, J. (2012). Cell wall constrains lateral diffusion of plant plasma-membrane proteins. Proceedings of the National Academy of Sciences of the United States of America **109,** 12805-12810.

Masserini, M., Palestini, P., and Freire, E. (1989). Influence of glycolipid oligosaccharide and long-chain base composition on the thermotropic properties of dipalmitoylphosphatidylcholine large unilamellar vesicles containing gangliosides. Biochemistry **28,** 5029-5034.

Matyash, V., Liebisch, G., Kurzchalia, T.V., Shevchenko, A., and Schwudke, D. (2008). Lipid extraction by methyl-tert-butyl ether for high-throughput lipidomics. Journal of lipid research **49,** 1137-1146.

Mongrand, S., Stanislas, T., Bayer, E.M., Lherminier, J., and Simon-Plas, F. (2010). Membrane rafts in plant cells. Trends in plant science **15,** 656-663.

Mongrand, S., Morel, J., Laroche, J., Claverol, S., Carde, J.P., Hartmann, M.A., Bonneu, M., Simon-Plas, F., Lessire, R., and Bessoule, J.J. (2004). Lipid rafts in higher plant cells: purification and characterization of Triton X-100-insoluble microdomains from tobacco plasma membrane. The Journal of biological chemistry **279,** 36277-36286.

Morel, J., Claverol, S., Mongrand, S., Furt, F., Fromentin, J., Bessoule, J.J., Blein, J.P., and Simon-Plas, F. (2006). Proteomics of plant detergent-resistant membranes. Molecular & cellular proteomics : MCP **5,** 1396-1411.

Mortimer, J.C., Yu, X., Albrecht, S., Sicilia, F., Huichalaf, M., Ampuero, D., Michaelson, L.V., Murphy, A.M., Matsunaga, T., Kurz, S., Stephens, E., Baldwin, T.C., Ishii, T., Napier, J.A., Weber, A.P., Handford, M.G., and Dupree, P. (2013). Abnormal glycosphingolipid mannosylation triggers salicylic acid-mediated responses in Arabidopsis. The Plant cell **25,** 1881-1894.

Mouritsen, O.G. (2010). The liquid-ordered state comes of age. Biochimica et biophysica acta **1798,** 1286-1288.

Noirot, E., Der, C., Lherminier, J., Robert, F., Moricova, P., Kieu, K., Leborgne-Castel, N., Simon-Plas, F., and Bouhidel, K. (2014). Dynamic changes in the subcellular distribution of the tobacco ROS-producing enzyme RBOHD in response to the oomycete elicitor cryptogein. Journal of experimental botany **65,** 5011-5022.

Pascher, I. (1976). Molecular arrangements in sphingolipids. Conformation and hydrogen bonding of ceramide and their implication on membrane stability and permeability. Biochimica et biophysica acta **455,** 433-451.

Pata, M.O., Hannun, Y.A., and Ng, C.K. (2010). Plant sphingolipids: decoding the enigma of the Sphinx. The New phytologist **185,** 611-630.

Quinn, P.J., and Wolf, C. (2009). The liquid-ordered phase in membranes. Biochimica et biophysica acta **1788,** 33-46.

Raffaele, S., Bayer, E., Lafarge, D., Cluzet, S., German Retana, S., Boubekeur, T., Leborgne-Castel, N., Carde, J.P., Lherminier, J., Noirot, E., Satiat-Jeunemaitre, B., Laroche-Traineau, J., Moreau, P., Ott, T., Maule, A.J., Reymond, P., Simon-Plas, F., Farmer, E.E., Bessoule, J.J., and Mongrand, S. (2009). Remorin, a solanaceae protein resident in membrane rafts and plasmodesmata, impairs potato virus X movement. The Plant cell **21,** 1541-1555.

Rehman, R.U., Stigliano, E., Lycett, G.W., Sticher, L., Sbano, F., Faraco, M., Dalessandro, G., and Di Sansebastiano, G.P. (2008). Tomato Rab11a characterization evidenced a difference between SYP121-dependent and SYP122-dependent exocytosis. Plant Cell Physiol **49,** 751-766.

Rennie, E.A., Ebert, B., Miles, G.P., Cahoon, R.E., Christiansen, K.M., Stonebloom, S., Khatab, H., Twell, D., Petzold, C.J., Adams, P.D., Dupree, P., Heazlewood, J.L., Cahoon, E.B., and Scheller, H.V. (2014). Identification of a sphingolipid alpha-glucuronosyltransferase that is essential for pollen function in Arabidopsis. The Plant cell **26,** 3314-3325.

Richards, R.L., Rao, M., Wassef, N.M., Glenn, G.M., Rothwell, S.W., and Alving, C.R. (1998). Liposomes containing lipid A serve as an adjuvant for induction of antibody and cytotoxic T-cell responses against RTS,S malaria antigen. Infection and immunity **66,** 2859-2865.

Rideal, J.T.D.a.E.K. (1963). Interfacial Phenomena (

Ripley, B.D. (1976). The second order analysis of stationary point process. Journal of Applied Probability **13,** 255-261.

Ruettinger, A., Kiselev, M.A., Hauss, T., Dante, S., Balagurov, A.M., and Neubert, R.H. (2008). Fatty acid interdigitation in stratum corneum model membranes: a neutron diffraction study. European biophysics journal : EBJ **37,** 759-771.

Scheffer, L., Solomonov, I., Weygand, M.J., Kjaer, K., Leiserowitz, L., and Addadi, L. (2005). Structure of cholesterol/ceramide monolayer mixtures: implications to the molecular organization of lipid rafts. Biophysical journal **88,** 3381-3391.

Shevchenko, A., and Simons, K. (2010). Lipidomics: coming to grips with lipid diversity. Nature reviews. Molecular cell biology **11,** 593-598.

Simon-Plas, F., Perraki, A., Bayer, E., Gerbeau-Pissot, P., and Mongrand, S. (2011). An update on plant membrane rafts. Current opinion in plant biology **14,** 642-649.

Simons, K., and Ikonen, E. (1997). Functional rafts in cell membranes. Nature **387,** 569-572.

Simons, K., and Toomre, D. (2000). Lipid rafts and signal transduction. Nature reviews. Molecular cell biology **1,** 31-39.

Simons, K., and Gerl, M.J. (2010). Revitalizing membrane rafts: new tools and insights. Nature reviews. Molecular cell biology **11,** 688-699.

Sonnino, S., and Prinetti, A. (2010). Gangliosides as regulators of cell membrane organization and functions. Advances in experimental medicine and biology **688,** 165-184.

Sperling, P., and Heinz, E. (2003). Plant sphingolipids: structural diversity, biosynthesis, first genes and functions. Biochimica et biophysica acta **1632,** 1-15.

Sperling, P., Franke, S., Luthje, S., and Heinz, E. (2005). Are glucocerebrosides the predominant sphingolipids in plant plasma membranes? Plant Physiol Biochem **43,** 1031-1038.

Subczynski, W.K., and Kusumi, A. (2003). Dynamics of raft molecules in the cell and artificial membranes: approaches by pulse EPR spin labeling and single molecule optical microscopy. Biochimica et biophysica acta **1610,** 231-243.

Tjellstrom, H., Hellgren, L.I., Wieslander, A., and Sandelius, A.S. (2010). Lipid asymmetry in plant plasma membranes: phosphate deficiency-induced phospholipid replacement is restricted to the cytosolic leaflet. FASEB journal : official publication of the Federation of American Societies for Experimental Biology **24,** 1128-1138.

Vitiello, F., and Zanetta, J.P. (1978). Thin-layer chromatography of phospholipids. Journal of chromatography **166,** 637-640.

Voxeur, A., and Fry, S.C. (2014). Glycosylinositol phosphorylceramides from Rosa cell cultures are boron-bridged in the plasma membrane and form complexes with rhamnogalacturonan II. The Plant journal : for cell and molecular biology **79,** 139-149.

Wang, W., Yang, X., Tangchaiburana, S., Ndeh, R., Markham, J.E., Tsegaye, Y., Dunn, T.M., Wang, G.L., Bellizzi, M., Parsons, J.F., Morrissey, D., Bravo, J.E., Lynch, D.V., and Xiao, S. (2008). An inositolphosphorylceramide synthase is involved in regulation of plant programmed cell death associated with defense in Arabidopsis. The Plant cell **20,** 3163-3179.

Worrall, D., Ng, C.K., and Hetherington, A.M. (2003). Sphingolipids, new players in plant signaling. Trends in plant science **8,** 317-320.

Yetukuri, L., Ekroos, K., Vidal-Puig, A., and Oresic, M. (2008). Informatics and computational strategies for the study of lipids. Molecular bioSystems **4,** 121-127.

FIGURE LEGENDS

Figure 1. Long chain (LCFA), very long chain (VLCFA) and 2-hydroxylated very long chain fatty acid (hVLCFA) content of tissue, microsomal, plasma membrane (PM) and Detergent-Insoluble Membranes (DIM) fractions from tobacco leaf or BY-2 cell culture

A, Fatty Acids were released from biological samples by acid methanolysis; the resulting FAMEs were subsequently derivatized with BSTFA before GC/MS analysis. The data are expressed as the mean of three independent experiments. LCFA: Long Chain Fatty Acid with 16, 18 or 20 carbon atoms, VLCFA: Very Long Chain Fatty Acid with 22 to 26 carbon atoms, hVLCFA, VLCFA with 22 to 26 carbon atoms hydroxylated in position 2; B, Histograms show the comparison between VLCFA and hVLCFA content of DIM and of GIPCs purified from tobacco leaves or BY-2 cell culture. The data are expressed as the mean of four independent experiments ±SD.

Figure 2. Analysis of GIPCs extracted from tobacco leaf and BY-2 cells by MALDI-MS and HP-TLC. Polyglycosylated GIPCs are enriched in DIMs

A, MALDI-MS analysis of GIPC extracts from BY-2 cells and tobacco leaf. Spectra were acquired in the negative ion mode using 2,6-dihydroxyacetophenone (DHA) as a matrix. GIPCs are grouped in series according to their number of saccharide units, from two (series A) to six (series E), see supplemental figure S7 for detailed analysis of the peaks; B, High Performance-Thin Layer Chromatography (HP-TLC) were used to separated the different series of GIPCs. Note that the series A show two bands called by Kaul and Lester 1975, PhytoSphingoLipid: PSL I and PSL II, corresponding to GlcNAc-GlcUA-IPC and $GlcNH_2$-GlcUA-IPC, respectively(Kaul and Lester, 1975). GIPCs extracted from *Arabidopsis thaliana* (*At*) and leek (*Ap.*, *Allium porrum*) were used as HP-TLC standards for series A and B respectively, according to (Cacas et al., 2013).

Figure 3. Quantification of polyglycosylated GIPCs found in PM and DIMs of BY-2 cells.

Quantification by HP-TLC coupled to GC-MS of polyglycosylated GIPCs found in PM and DIMs of BY-2 cells. The data are expressed as the mean of three independent experiments as the percentage of total GIPCs found in PM and DIMs respectively ±SD.

Figure 4. Lipid content of tobacco leaf (A.) and BY-2 cell (B.) PM and DIMs

Left: From the results presented in Fig. 1 and 2 and those obtained on phospholipids and sterols on the same plant materials (Furt et al., 2010), we were able to determine the lipid content of PM and DIM expressed as mol%. *Right*, The three main classes of lipids, namely phospholipids, sterols and sphingolipids were summed and represented as mol% of total lipids. The data are expressed as means of three independent experiments ± SD. Abbreviations are as followed: phosphatidylethanolamine (PE), phosphatidylcholine (PC), phosphatidic acid (PA), phosphatidylinositol (PI), phosphatidylinositol 4-phosphate (PI4P), phosphatidylinositol 4,5-bisphosphate (PI4,5P_2), digalactosyldiacylglycerol (DGDG), Steryl-glucosides (SG), Acyl Steryl-glucosides (ASG), free sterols (Sterols), glucosylceramides (GluCER), GlycosylInositolPhosphorylCeramides (GIPCs).

Right: sum of percentage of glycerolipids (PE, PC, PA, PI, PIP4P, PI4,5P_2, DGDG) sterols (free sterols, SG, ASG) and sphingolipids (gluCER, GIPCs).

Figure 5. Test for the specificity of antibodies to polyglycosylated GIPCs

A, Home–made PVDF dot-blots were done with DEAE fractions of GIPC purification, see supplemental Fig. S11. PVDF membranes were blotted with pre-immun serum (1/100) or with 53 days serum (1/100) immunized against polyglycosylated GIPCs, see experimental section; B, Lipids from BY-2 cell PM were separated on HP-TLC. The plates were blotted with pre-immun serum (1/100) or with 53 days serum (1/100) immunized against polyglycosylated GIPCs, see experimental section.

Figure 6. Polyglycosylated GIPCs locates in nanoscale membrane domains on BY-2 cell PM vesicles. A, Transmission electron micrographs of negatively stained tobacco PM vesicles immunogold labeled on grids with purified antibodies to polyglycosylated

GIPCs detected by 6 nm colloidal gold conjugated goat anti-rabbit. Circles indicate obvious membrane domains; Bars = 20 nm; B Total number of 49 independent gold-labeled PM vesicles were analyzed for the statistics; C; Ripley's K-function analysis of GIPCs distribution on the surface of PM vesicles: y axis K(r) is the average number of particles lying at a distance less than r (x axis), normalized by the mean particle density. This Ripley's analysis of the labeled PM vesicles (black line) indicates clustering of the gold particles when compared to a theoretical simulation for a completely random (Poisson) point pattern (red dotted line).

Figure 7. Effect on membrane order level of tobacco leaf or BY-2 cell purified GIPCs, in combination with phospholipids and free sterols.

The Red/Green Mean ratio of the membrane (RGM) of 1µm diameter LUVs of different compositions labeled with di-4ANEPPDHQ (3 µM) was measured by spectrofluorimetry in the presence of GIPCs isolated from tobacco BY-2 cells or tobacco leaves. Data shown are mean values ± SD, n=5 or more independent repetitions. The different letters indicate significantly different values (p-value < 0.05).

Figure 8. Surface pressure-area (Π-A) isotherms, at the air-aqueous phase interface, of pure GIPC (○) and sitosterol (□) monolayers and of mixed GIPC/sitosterol monolayer (△) prepared at GIPC a 0.85 molar ratio.

A, The isotherms were recorded at 22 ± 1°C with an aqueous subphase composed by a Tris 10mM buffer at pH 7.0. Duplicate experiments using independent preparations yielded similar results; B, Comparison of the experimental (white bars) and theoretical (black bars) mean molecular areas at a surface pressure of 10 mN/m, 20 mN/m and 30 mN/m for GIPC/sitosterol at a 0.85 GIPC molar ratio. The theoretical value is obtained according to the additivity rule : $A_{12} = A_1X_1 + A_2X_2$ where A_{12} is the mean molecular area for ideal mixing of the two components at a given Π, A_1, and A_2 are the molecular areas of the respective components in their pure monolayers at the same Π and X_1 and X_2 are the molar ratios of components 1 and 2 in the mixed monolayers; C, Excess free energy of mixing (ΔG^{ex}) (white bars), and free energy of mixing (ΔG^{M}) (black bars) of the mixed monolayer GIPC/sitosterol at a 0.85 molar ratio of GIPC for various surface

1197 pressures. ΔG^{ex} and ΔG^{M} were calculated according to the following equations (Maget-
1198 Dana, 1999) (Eeman et al., 2005) : $\Delta G^{ex} = \int_0^{\Pi} A_{12}\, d\Pi - X_1 \int_0^{\Pi} A_1\, d\Pi - X_2 \int_0^{\Pi} A_2\, d\Pi$ where A is
1199 the mean molecular area, X is the molar fraction, subscripts 1 and 2 refer, respectively, to
1200 pure components 1 and 2 and 12 to their mixtures, and $\Delta G^{M} = \Delta G^{ex} + \Delta G^{id}$ where ΔG^{id} is
1201 the free energy for ideal mixing and can be calculated from the following equation,
1202 $\Delta G^{id} = RT\left(X_1 \ln X_1 + X_2 \ln X_2\right)$ where R is the universal gas constant and T the absolute
1203 temperature.
1204
1205 **Figure 9. Modeling approaches**
1206 A, Theoretical interactions between 8 GIPC and 8 sitosterol molecules calculated by HM
1207 docking method. Sitosterol molecules are in green and GIPCs are coloured with carbon
1208 atoms in grey, oxygen in red, phosphorus in purple, nitrogen in blue and hydrogen in
1209 white; B, Most stable insertion of gluCER d18:2/h16:0 (left) and GIPCs t18:0/h24:0
1210 (Frazier and Alber, 2012) into an implicit bilayer calculated by IMPALA. The yellow
1211 plane represents the center of the bilayer; the mauve plane stands for the lipid polar
1212 head/acyl chain interface and the pink plane, for the water/lipid polar head interface; C,
1213 Interaction energies calculated for GIPCs and GIPCs/sitosterol (from Fig. 9A)
1214 monolayers. Epolar corresponds to polar and electrostatic interactions and Epho and
1215 Evdw, to hydrophobic and Van der Waals interactions, respectively. The mean calculated
1216 interfacial molecular areas for GIPCs alone or in interaction with sitosterol are also
1217 indicated.
1218
1219 **Figure 10. Model for the organization of lipids in tobacco plasma membrane.**
1220 To build this model, we took the molar composition of the BY-2 PM obtained in Fig. 4
1221 and used the data obtained by Tjellstrom and collaborators 2010, who were able to
1222 calculate the distribution of cytosolic/apoplastic lipids. We hypothesize that GIPCs are
1223 located exclusively in the apoplastic face, see text.
1224

Supplemental Data

The following materials are available in the online version of this article.

Supplemental Figure S1. Typical GC-MS spectrogram of total FAMES and sterols extracted from BY-2 cell PM. Two internal standards (IS) were added to quantify GIPC: 2-hydroxylated 14 carbon atom fatty acid (h14), and heptadecanoic acid (17:0).

Supplemental Figure S2. Fatty acid content of tissue, microsomal, plasma membrane (PM) and Detergent-Insoluble Membranes (DIM) fractions from tobacco leaves or BY-2 cell culture. A. Fatty Acids were released from biological samples by acid methanolysis; the resulting FAMEs were subsequently derivatized with BSTFA before GC/MS analysis. LCFA: Long Chain Fatty Acid with 16, 18 or 20 carbon atoms, VLCFA: Very Long Chain Fatty Acid with 22 to 26 carbon atoms, hVLCFA, 2-hydroxylated Very Long Chain Fatty Acid with 22 to 26 carbon atoms. The data are expressed as the mean of three independent experiments ± SEs (Garssen et al.).
B. Sum of LCFA: Long Chain Fatty Acid with 16, 18 or 20 carbon atoms, VLCFA: Very Long Chain Fatty Acid with 22 to 26 carbon atoms, hVLCFA, 2-hydroxylated Very Long Chain Fatty Acid with 22 to 26 carbon atoms expressed as nmol of FAMES per mg of proteins. The data are expressed as the mean of three independent experiments ± SEs (Garssen et al.).

Supplemental Figure S3. Fatty acid content of Detergent-Insoluble Membranes (DIM) *vs.* Detergent-Soluble Membranes (DSM) from tobacco leaf purified PM. Fatty Acids were released by acid methanolysis; the resulting FAMEs were subsequently derivatized with BSTFA before GC/MS analysis. LCFA: Long Chain Fatty Acid with 16, 18 or 20 carbon atoms, VLCFA: Very Long Chain Fatty Acid with 22 to 26 carbon atoms, hVLCFA, 2-hydroxylated Very Long Chain Fatty Acid with 22 to 26 carbon atoms. The data are expressed as the mean of three independent experiments ± SEs (Garssen et al.).

Supplemental Figure S4. Fatty acid and sterol content of purified Acyl Steryl Glucosides (ASG) extracted from tobacco leaves or BY-2 cell culture. ASG was purified by HP-TLC (Lefebvre et al., 2007), scratched from the silica and submitted to either acid methanolysis for FAMES analysis, or to saponification for sterol analysis. After TMS derivatizasion, FAMES and sterols were quantified by GC-MS. The data are expressed as the mean of three independent experiments ± SEs (Garssen et al.).

Supplemental Figure S5. Fatty acid content of purified glucosyl ceramide (gluCER) extracted from tobacco leaves or BY-2 cell culture and purified by TLC. GluCER was purified by HP-TLC (Lefebvre et al., 2007), scratched from the silica and submitted to acid methanolysis for FAMES analysis, After BSTFA derivatizasion, FAMES were quantified by GC-MS. The data are expressed as the mean of three independent experiments ± SEs (Garssen et al.).

Supplemental Figure S6. LCB content of GIPCs, plasma membrane (PM) and Detergent-Insoluble Membranes (DIM) from tobacco leaves or BY-2 cell culture. A, LCBs were isolated by hydrolysis from GIPCs purified from leaf and BY-2 cells, converted to their fatty aldehydes by peroxydation and separated by GC, as described (Cacas et al., 2012a); B-C, LCBs content were determined in PM and DIM purified from tobacco leaves and BY-2 cells. Abbreviations are as follow: Peak nomenclature in the key is systematically based upon the 2-amino-acyl backbone of the LCB. t18:0: 2-aminooctadecane-1,2,4-triol (trivial name phytosphingosine); t18:1(8Z): (Z)-2-aminooctadec-8-ene-1,2,4-triol, (trivial name (8Z)-phytosphingenine); d18:1(4E): (E)-2-aminooctadec-4-ene-1,2-diol (trivial name sphingosine); d18:2(4E/8Z,E): (E,Z)-2-aminooctadeca-4,8-dienine-1,2-diol (trivial name (4E,8Z)-sphingadienine); d18:0: 2-aminooctadecane-1,2-diol (trivial name sphinganine).

Supplemental Figure S7. MALDI-MS analysis of GIPC extracts from BY-2 cells. Spectra were acquired in the negative ion mode using 2,6-dihydroxyacetophenone (DHA) as a matrix. GIPCs are grouped in series according to their number of saccharide units, from two sugars (series A) to six (series E).

Supplemental Figure S8. MALDI-MS analysis of GIPC extracts purified from PM and DIMs extracted from tobacco leaves. Spectra were acquired in the negative ion mode using 2,6-dihydroxyacetophenone (DHA) as a matrix.

Supplemental Figure S9. Determination of lipid-to-protein ratio in plant PM. A, 100 µg of BY-2 cell purified PM were extracted by protocol #1 (see experimental procedures) using chloroform/methanol/HCl, the aqueous phase were re-extracted by buranol-1. Histograms shows the total FA content recovered in each solvent fractions expressed as the mean ± SD of three independent experiments, compare with the direct transesterification of 100 µg of BY-2 cell purified PM.

Supplemental Figure S10. Fatty acid content of total lipids from grape cell culture. A, Fatty Acids were released from biological samples by acid methanolysis; the resulting FAMEs were subsequently derivatized with BSTFA before GC/MS analysis. LCFA: Long Chain Fatty Acid with 16, 18 or 20 carbon atoms, VLCFA: Very Long Chain Fatty Acid with 22 to 26 carbon atoms, hVLCFA, 2-hydroxylated Very Long Chain Fatty Acid with 22 to 26 carbon atoms. The data are expressed as the mean of three independent experiments ± SEs (Garssen et al.); B, Lipids from grape cell culture were extracted with or without preliminary hot isopropanol treatment. Polar lipis are further separated by HP-TLC by the solvent migration described in (Vitiello and Zanetta, 1978). Abbreviations are as described in Fig. 3; C, Rationale for the three lipid extraction protocols; D, Fatty acid analyses of lyophilized grape cell culture by the three lipid extraction protocols with or without hot isopropanol pre-treatment, compare with the direct transesterification of grape cell culture (TOTAL, *left*). The data are expressed as means of three independent experiments ± SD.

Supplemental Figure S11. Purification of GIPCs from BY-2 cells by DEAE chromatography. A, Total BY-2 cell GIPC were separated by DEAE. The different fractions were eluted with increasing amount of ammonium acetate: fractions 9-49, see material and methods. The purification process was monitored by on HP-TLC. Lipids

were visualized by spraying plates with primuline. $GIPC^{BY2}$ are the starting material used as control standards for HP-TLC; B, Purified and dialyzed fractions (GIPC series A and B-F) were check for purifty by HP-TLC and MALDI-MS. Note the absence of residual glycerolipids and sterols, and the strong enrichment of series A in one hand (*middle*) and series B-F in the other hand.

Supplemental Figure S12. Test by ELISA of the specificity of antibodies against polyglycosylated GIPCs. ELISA were performed using BSA as negative control. Data represent mean value of four technical replicates. Vertical bars indicate standard error of the mean.

Supplemental Figure S13. Cross reactivity of antibodies against polyglycosylated GIPCs. A, The cross reactivity of antibodies against polyglycosylated GIPCs was performed on "PIP strips" according to manufacturers's instructions (Echelon Bioscience, USA; http://www.echelon-inc.com). Membranes were first incubated with rabbit antibodies against polyglycosylated GIPCs (dilution 1/100 for 1h at RT) and further with horseradish peroxydase-conjugated secondary anti mouse antibody (dilution 1/15,000 for 1h at RT); B, A negative control with preimmume serum, or without primary antibodies is shown at the bottom panel; C, Positive control is performed with antibodies against PI4,5P2 (Antibodies against native PI4,5P2 from bovine spinal cord (www.Assay designs.com); dilution 1/1,000 for 1h at RT). Note that these antibodies are 10-fold more diluted than antibodies against polyglycosylated GIPCs.

Supplemental Figure S14. Immumogold labeling controls of PM vesicles.

A, omission of the primary antibody; B, use of the pre-immune serum of rabbit used for immunization of polyglycosylated GIPCs with the preimmune serum of rabbit used for immunization of polyglycosylated GIPCs; C, with antibodies against the proton pump ATPase PMA as used in (Raffaele et al., 2009)

Figure 1

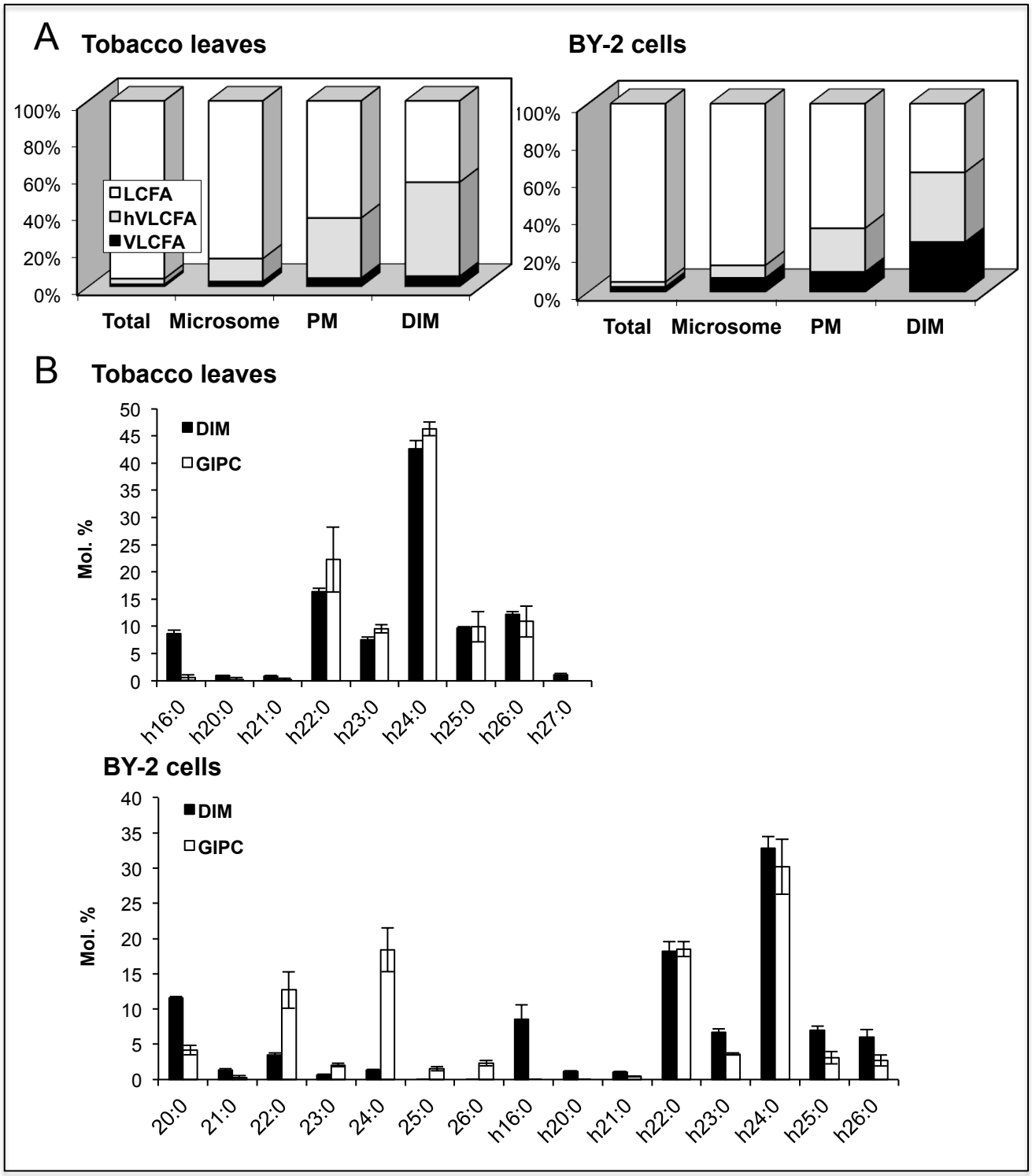

Figure 1. Long chain (LCFA), very long chain (VLCFA) and 2-hydroxylated very long chain fatty acid (hVLCFA) content of tissue, microsomal, plasma membrane (PM) and Detergent-Insoluble Membranes (DIM) fractions from tobacco leaf or BY-2 cell culture

A, Fatty Acids were released from biological samples by acid methanolysis; the resulting FAMEs were subsequently derivatized with BSTFA before GC/MS analysis. The data are expressed as the mean of three independent experiments. LCFA: Long Chain Fatty Acid with 16, 18 or 20 carbon atoms, VLCFA: Very Long Chain Fatty Acid with 22 to 26 carbon atoms, hVLCFA, VLCFA with 22 to 26 carbon atoms hydroxylated in position 2;

B, Histograms show the comparison between VLCFA and hVLCFA content of DIM and of GIPCs purified from tobacco leaves or BY-2 cell culture. The data are expressed as the mean of four independent experiments ±SD.

Figure 2

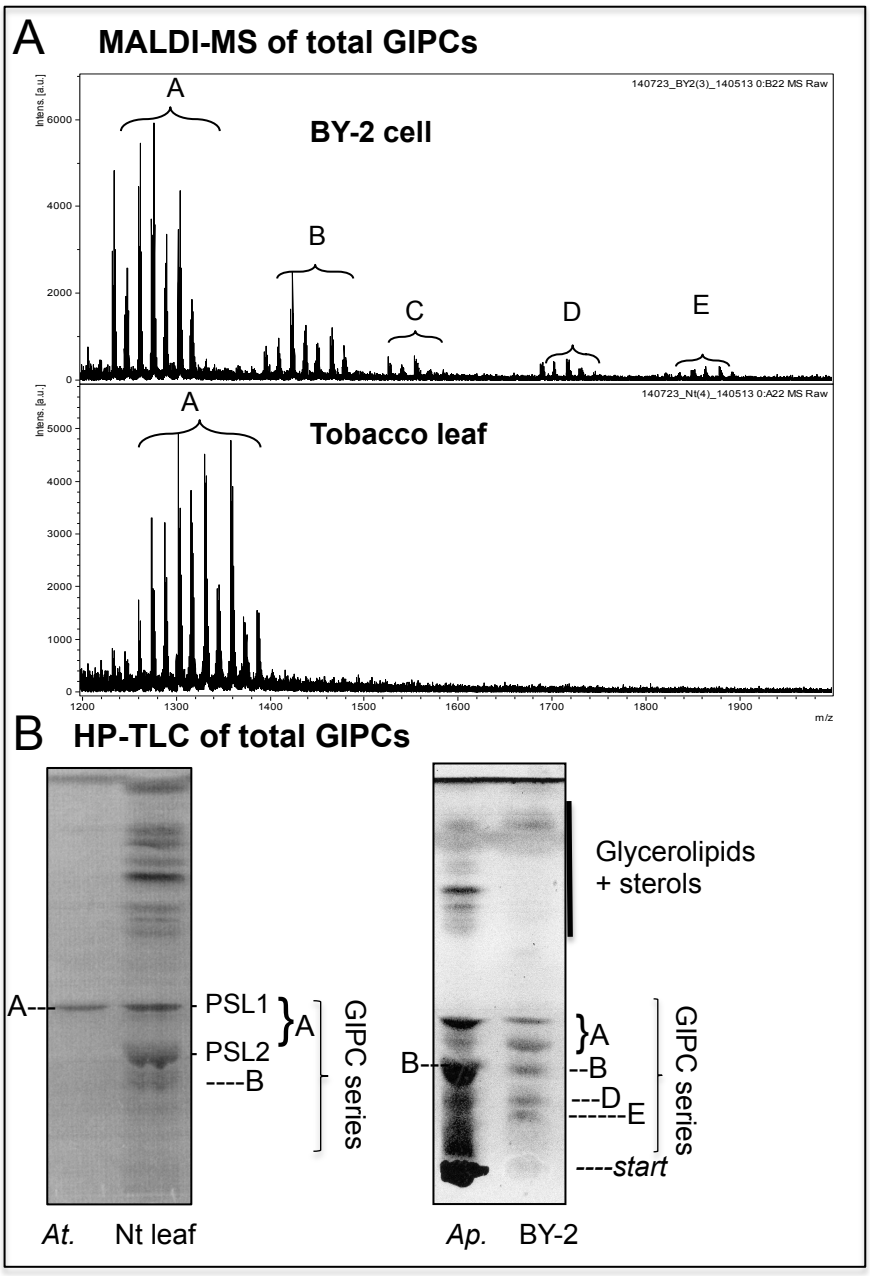

Figure 2. Analysis of GIPCs extracted from tobacco leaf and BY-2 cells by MALDI-MS and HP-TLC. Polyglycosylated GIPCs are enriched in DIMs

A, MALDI-MS analysis of GIPC extracts from BY-2 cells and tobacco leaf. Spectra were acquired in the negative ion mode using 2,6-dihydroxyacetophenone (DHA) as a matrix. GIPCs are grouped in series according to their number of saccharide units, from two (series A) to six (series E), see supplemental figure S7 for detailed analysis of the peaks;

B, High Performance-Thin Layer Chromatography (HP-TLC) were used to separated the different series of GIPCs. Note that the series A show two bands called by Kaul and Lester 1975, PhytoSphingoLipid: PSL I and PSL II, corresponding to GlcNAc-GlcUA-IPC and $GlcNH_2$-GlcUA-IPC, respectively(Kaul and Lester, 1975). GIPCs extracted from *Arabidopsis thaliana* (*At*) and leek (*Ap.*, *Allium porrum*) were used as HP-TLC standards for series A and B respectively, according to (Cacas et al., 2013).

Figure 3

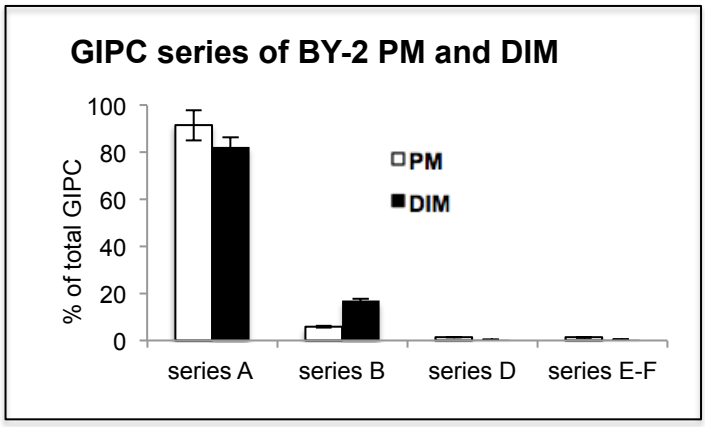

Figure 3. Quantification of polyglycosylated GIPCs found in PM and DIMs of BY-2 cells.
Quantification by HP-TLC coupled to GC-MS of polyglycosylated GIPCs found in PM and DIMs of BY-2 cells. The data are expressed as the mean of three independent experiments as the percentage of total GIPCs found in PM and DIMs respectively ±SD.

Figure 4

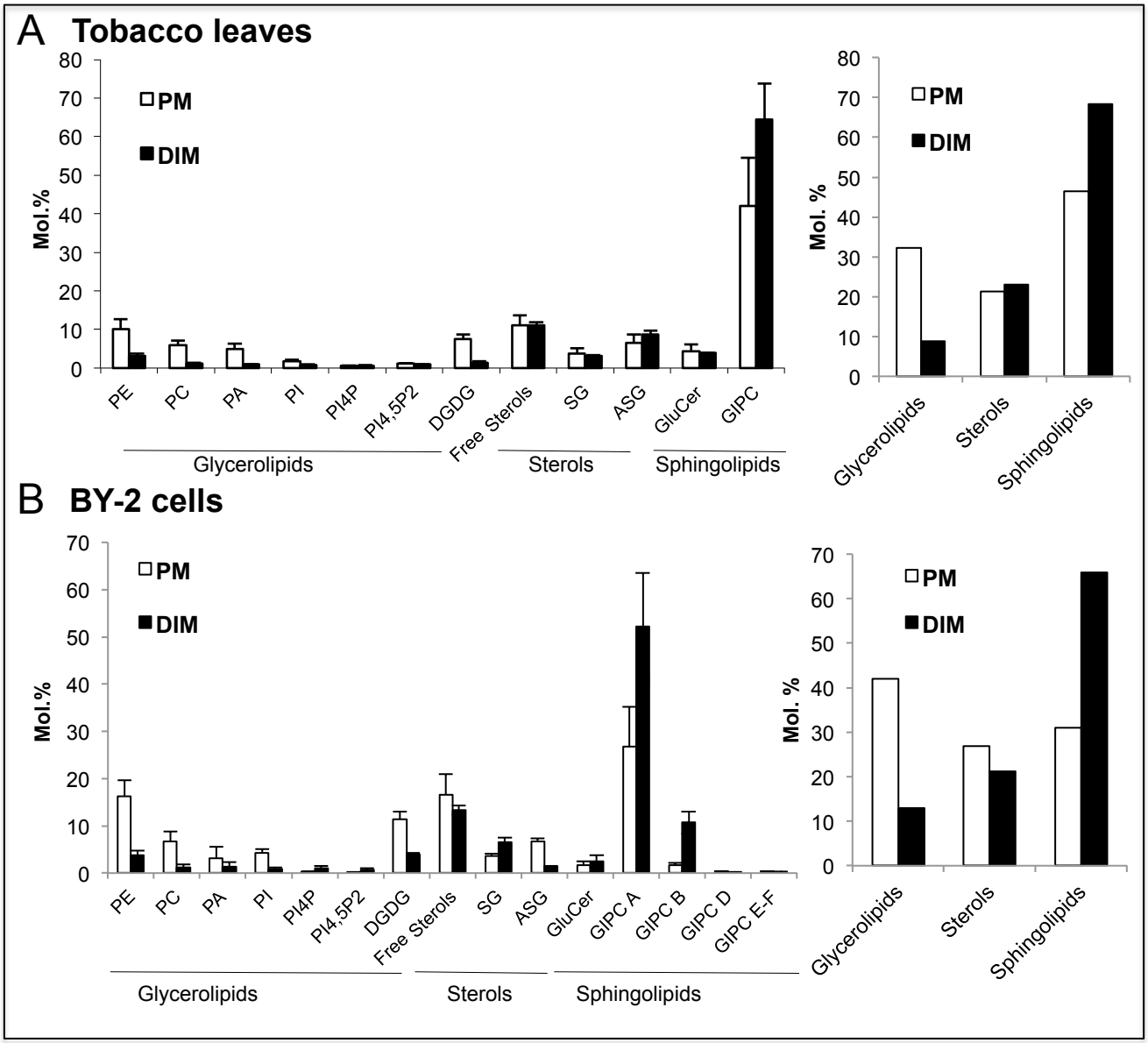

Figure 4. Lipid content of tobacco leaf (A.) and BY-2 cell (B.) PM and DIMs
Left: From the results presented in Fig. 1 and 2 and those obtained on phospholipids and sterols on the same plant materials (Furt et al., 2010), we were able to determine the lipid content of PM and DIM expressed as mol%. *Right*, The three main classes of lipids, namely phospholipids, sterols and sphingolipids were summed and represented as mol% of total lipids. The data are expressed as means of three independent experiments ± SD. Abbreviations are as followed: phosphatidylethanolamine (PE), phosphatidylcholine (PC), phosphatidic acid (PA), phosphatidylinositol (PI), phosphatidylinositol 4-phosphate (PI4P), phosphatidylinositol 4,5-bisphosphate (PI4,5P_2), digalactosyldiacylglycerol (DGDG), Steryl-glucosides (SG), Acyl Steryl-glucosides (ASG), free sterols (Sterols), glucosylceramides (GluCER), GlycosylInositolPhosphorylCeramides (GIPCs).
Right: sum of percentage of glycerolipids (PE, PC, PA, PI, PIP4P, PI4,5P_2, DGDG) sterols (free sterols, SG, ASG) and sphingolipids (gluCER, GIPCs).

Figure 5

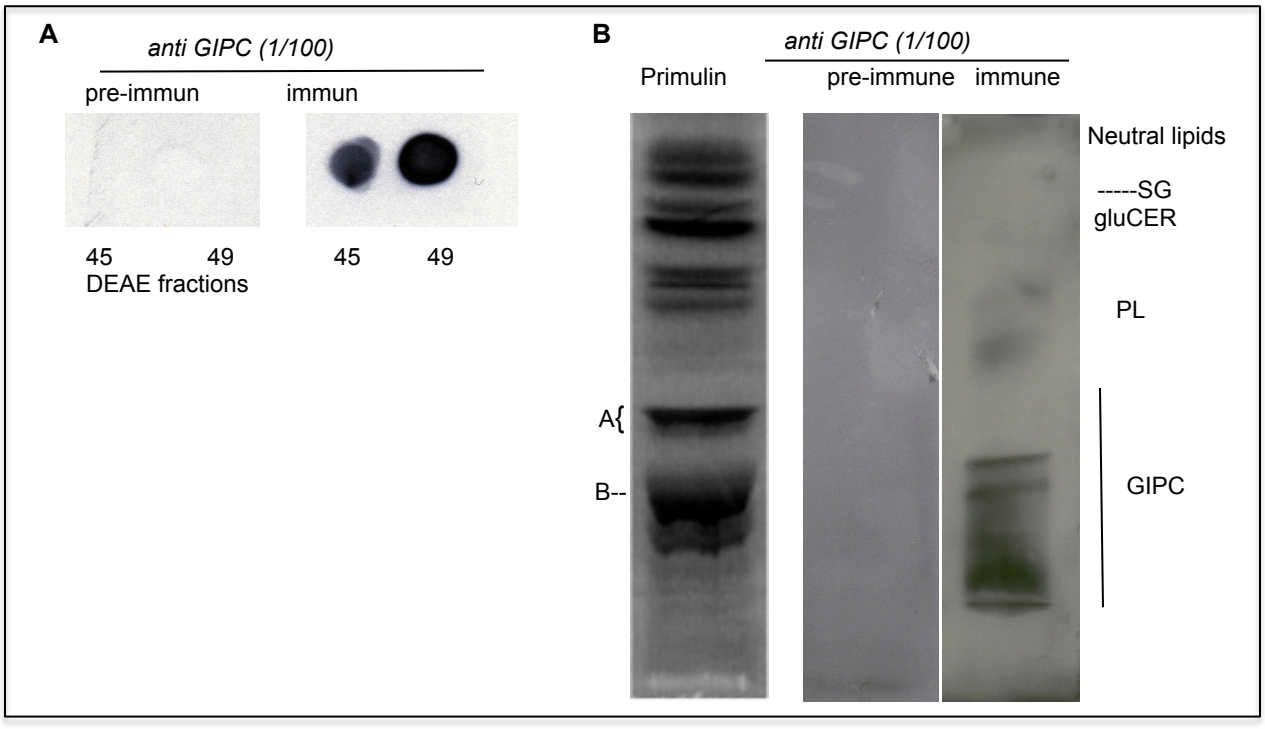

Figure 5. Test for the specificity of antibodies to polyglycosylated GIPCs
A, Home–made PVDF dot-blots were done with DEAE fractions of GIPC purification, see supplemental Fig. S10. PVDF membranes were blotted with pre-immun serum (1/100) or with 53 days serum (1/100) immunized against polyglycosylated GIPCs, see experimental section; B, Lipids from BY-2 cell PM were separated on HP-TLC. The plates were blotted with pre-immun serum (1/100) or with 53 days serum (1/100) immunized against polyglycosylated GIPCs, see experimental section.

Figure 6

A Immunogold labeling on PM vesicles with antibodies to polyglycosylated GIPCs

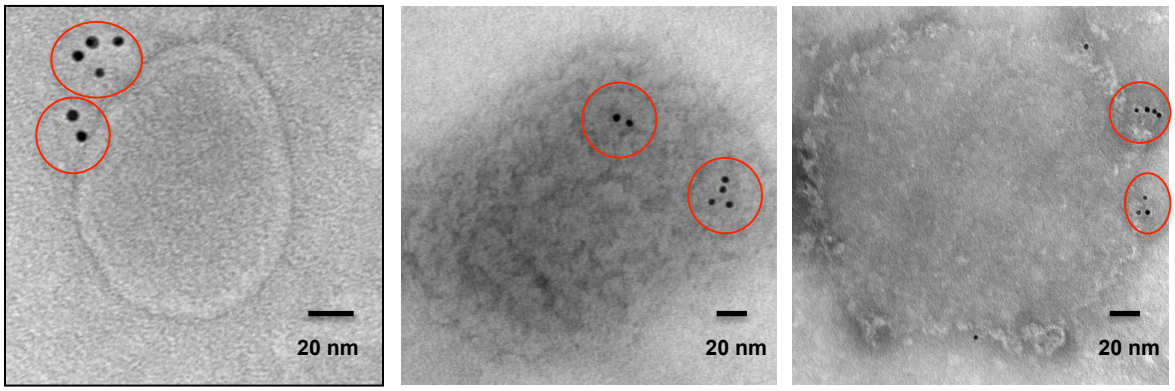

B Statistical analysis

Cluster size of vesicles with 3 gold particles and higher	34.5 ± 7.8nm
Average diameter of PM vesicles	246.3 nm
Average PM vesicle area	0,047 µm²
Average number of gold per PM vesicle	6.9
Average number of gold particles per cluster	4.1
Distance between two neighboring clusters	> 20 nm

C Ripley's Function analysis of GIPCs distribution

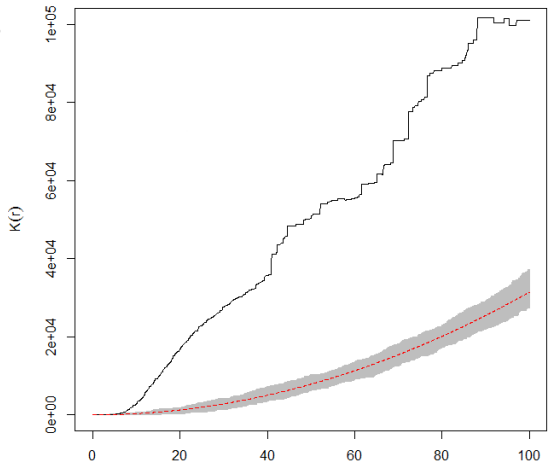

Figure 6. Polyglycosylated GIPCs locates in nanoscale membrane domains in BY-2 cell PM vesicles. A, Transmission electron micrographs of negatively stained tobacco PM vesicles immunogold labeled on grids with purified antibodies to polyglycosylated GIPCs detected by 6 nm colloidal gold conjugated goat anti-rabbit. Circles indicate obvious membrane domains; Bars = 20 nm; B, Total number of 49 independent gold-labeled PM vesicles were analyzed for the statistics; C, Ripley's K-function analysis of GIPCs distribution on the surface of PM vesicles: y axis (K(r) is the average number of particles lying at a distance less than r (x axis) from a typical particle, normalized by the mean particle density. This Ripley's analysis of the labeled PM vesicles (black line) indicates clustering of the gold particles when compared to a theoretical simulation for a completely random (Poisson) point pattern (red dotted line).

Figure 7

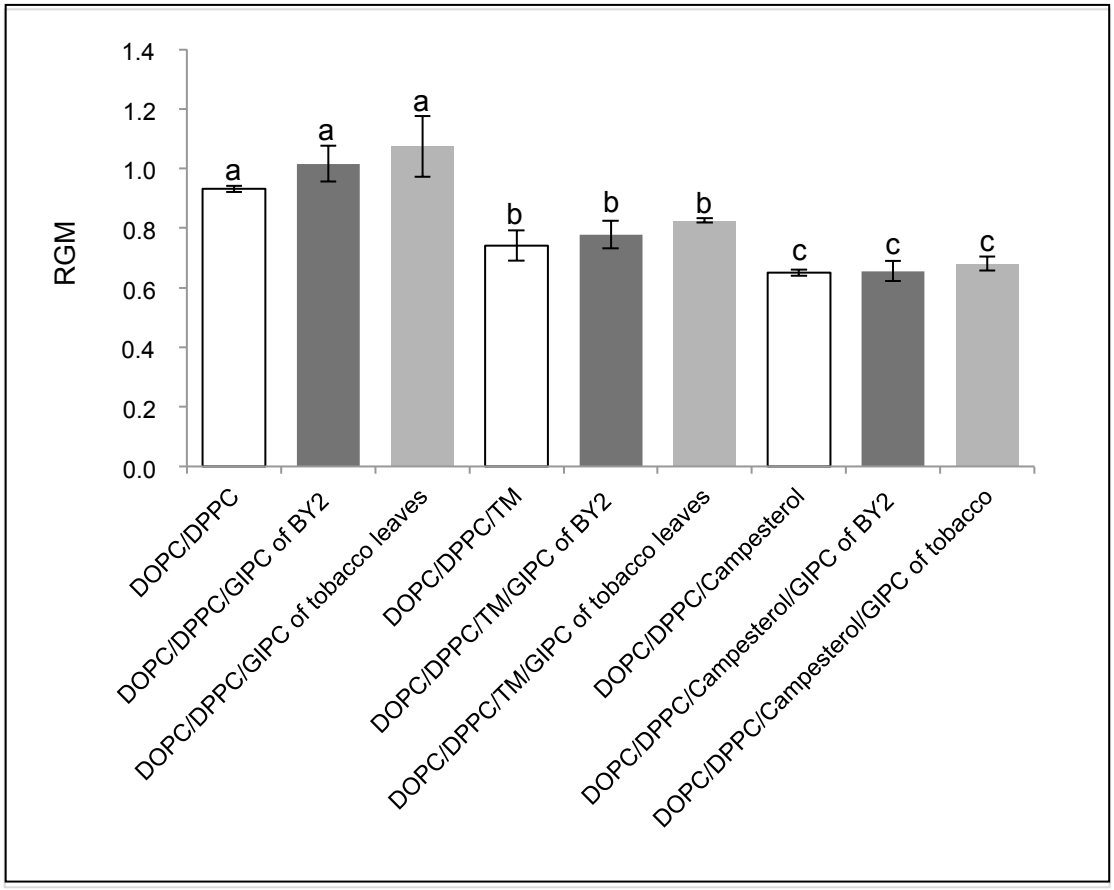

Figure 7. Effect on membrane order level of tobacco leaf or BY-2 cell purified GIPCs, in combination with phospholipids and free sterols.

The red/green ratio (Nichols et al.) of 1µm diameter LUVs of different compositions labeled with di-4ANEPPDHQ (3 µM) was measured by spectrofluorimetry in the presence of GIPCs isolated from tobacco BY-2 cells or tobacco leaves. Data shown are mean values ± SD, n=5 or more independent repetitions. The different letters indicate significantly different values (p-value < 0.05). RGM: Red/ Green Mean ratio of the membrane.

Figure 8

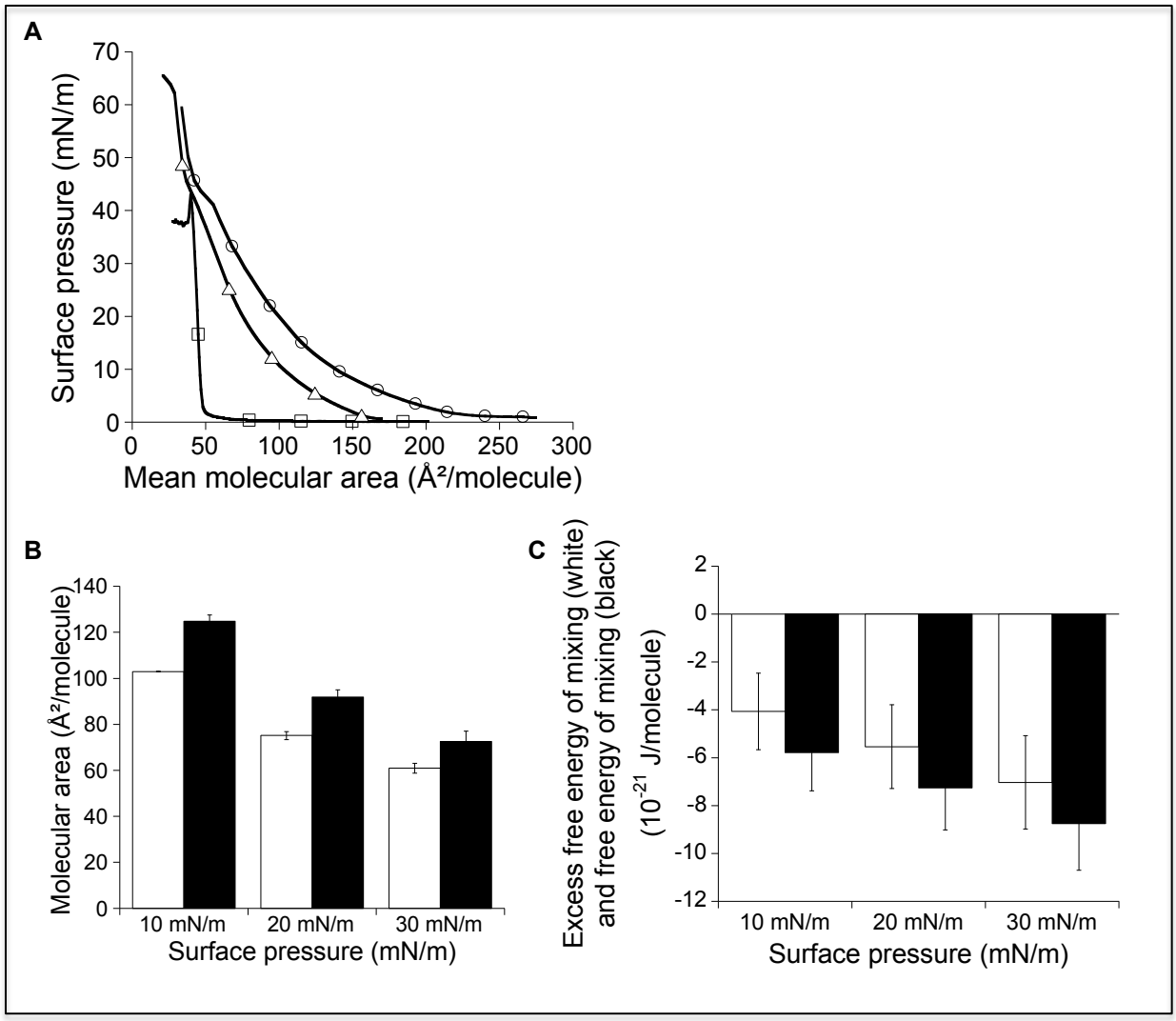

Figure 8. Surface pressure-area (Π-A) isotherms, at the air-aqueous phase interface, of pure GIPC (○) and sitosterol (□) monolayers and of mixed GIPC/sitosterol monolayer (△) prepared at GIPC a 0.85 molar ratio.

A, The isotherms were recorded at 22 ± 1°C with an aqueous subphase composed by a Tris 10mM buffer at pH 7.0. Duplicate experiments using independent preparations yielded similar results;

B, Comparison of the experimental (white bars) and theoretical (black bars) mean molecular areas at a surface pressure of 10 mN/m, 20 mN/m and 30 mN/m for GIPC/sitosterol at a 0.85 GIPC molar ratio. The theoretical value is obtained according to the additivity rule : $A_{12} = A_1X_1 + A_2X_2$ where A_{12} is the mean molecular area for ideal mixing of the two components at a given Π, A_1, and A_2 are the molecular areas of the respective components in their pure monolayers at the same Π and X_1 and X_2 are the molar ratios of components 1 and 2 in the mixed monolayers; C, Excess free energy of mixing (DG^{ex}) (white bars), and free energy of mixing (DG^{M}) (black bars) of the mixed monolayer GIPC/sitosterol at a 0.85 molar ratio of GIPC for various surface pressures. DG^{ex} and DG^{M} were calculated according to the following equations (Maget-Dana, 1999) (Eeman et al., 2005) : where A is the mean molecular area, X is the molar fraction, subscripts 1 and 2 refer, respectively, to pure components 1 and 2 and 12 to their mixtures, and where DG^{id} is the free energy for ideal mixing and can be calculated from the following equation, where R is the universal gas constant and T the absolute temperature.

Figure 9

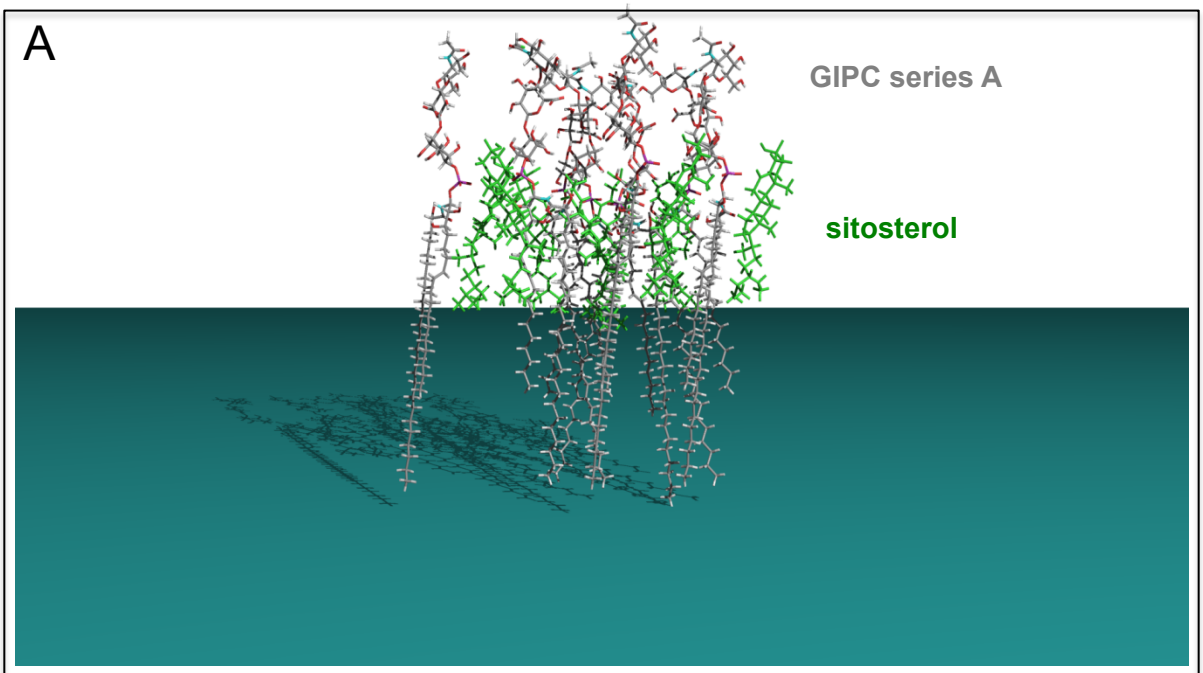

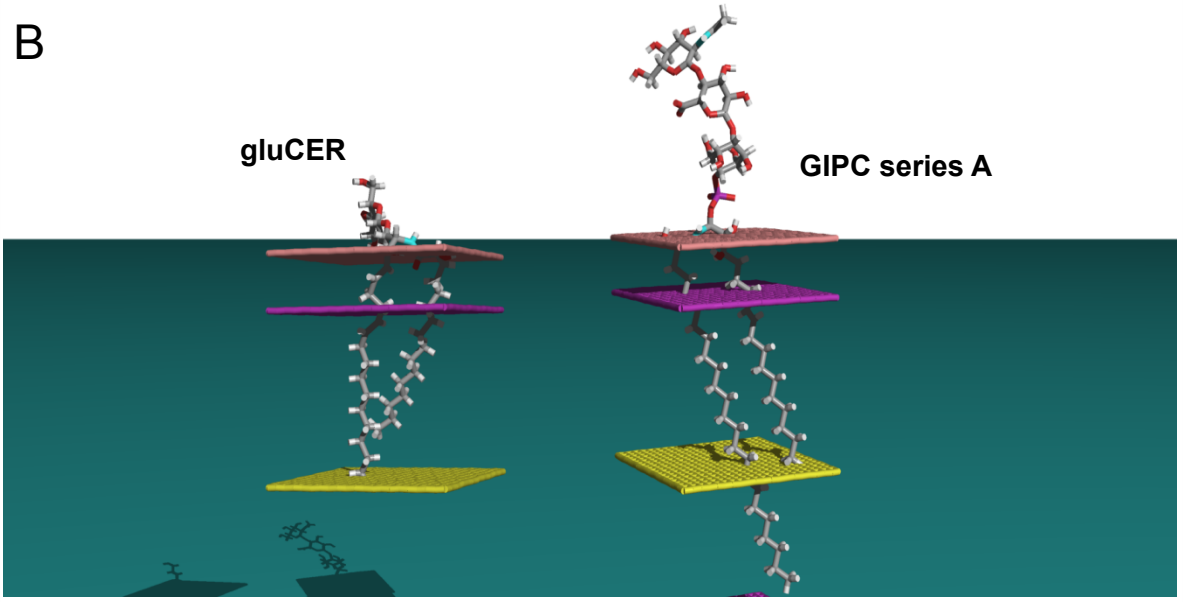

C

Molecule	E^{tot}	E^{vdw}	E^{polar}	E^{pho}	Mean area ($Å^2$)
GIPC	-23.5±2	-7.1±1	-2.3±0.4	-14.1±1.2	68.8±10
GIPC/sitosterol	-20.9±1.3	-10.2±1	-0.4±0.1	-10.3±1.1	57.6±8

Figure 9. Modeling approaches
A, Theoretical interactions between 8 GIPC and 8 sitosterol molecules calculated by HM docking method. Sitosterol molecules are in green and GIPCs are coloured with carbon atoms in grey, oxygen in red, phosphorus in purple, nitrogen in blue and hydrogen in white; B, Most stable insertion of gluCER d18:2/h16:0 (left) and GIPCs t18:0/h24:0 (Frazier and Alber, 2012) into an implicit bilayer calculated by IMPALA. The yellow plane represents the center of the bilayer; the mauve plane stands for the lipid polar head/acyl chain interface and the pink plane, for the water/lipid polar head interface; C, Interaction energies calculated for GIPCs and GIPCs/sitosterol (from Fig. 9A) monolayers. Epolar corresponds to polar and electrostatic interactions and Epho and Evdw, to hydrophobic and Van der Waals interactions, respectively. The mean calculated interfacial molecular areas for GIPCs alone or in interaction with sitosterol are also indicated.

Figure 10

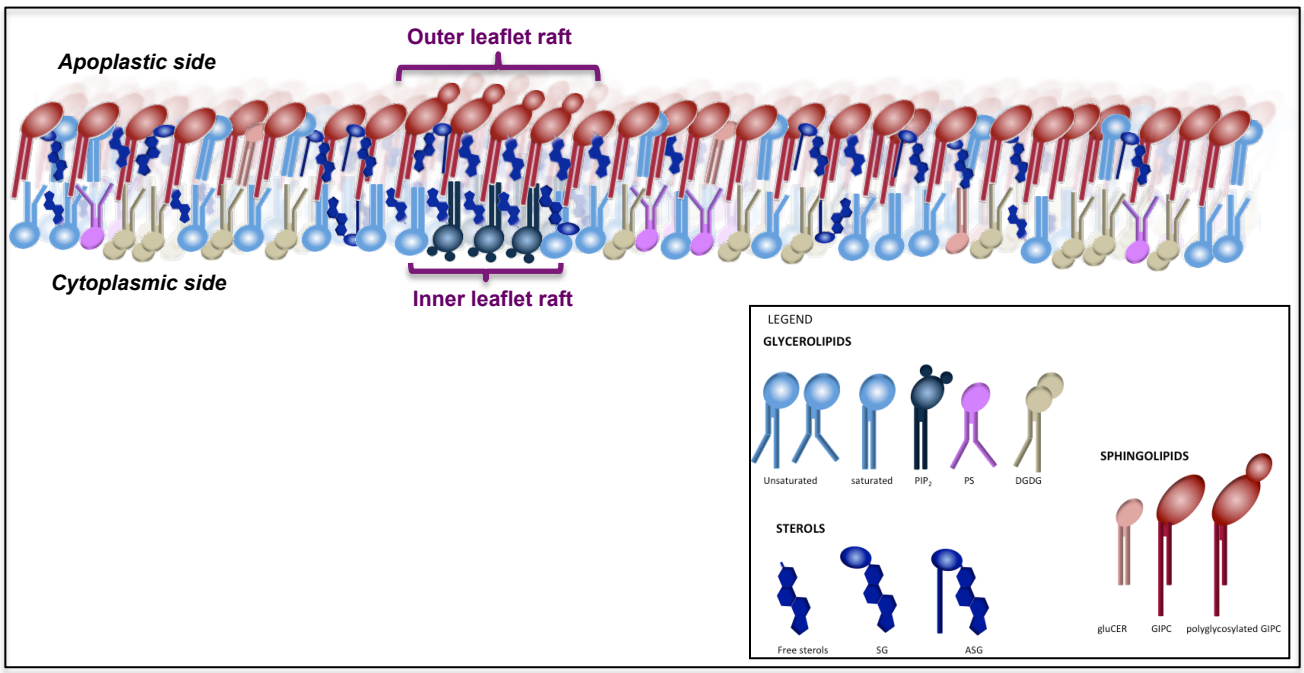

Figure 10. Model for the organization of lipids in tobacco plasma membrane.
To build this model, we took the molar composition of the BY-2 PM obtained in Fig. 4 and used the data obtained by Tjellstrom and collaborators 2010, who were able to calculate the distribution of cytosolic *vs*. apoplastic lipids. We hypothesize that GIPCs are located exclusively in the apoplastic face, see text.

Parsed Citations

Bensikaddour, H., Fa, N., Burton, I., Deleu, M., Lins, L., Schanck, A., Brasseur, R., Dufrene, Y.F., Goormaghtigh, E., and Mingeot-Leclercq, M.P. (2008). Characterization of the interactions between fluoroquinolone antibiotics and lipids: a multitechnique approach. Biophysical journal 94, 3035-3046.
Pubmed: Author and Title
CrossRef: Author and Title
Google Scholar: Author Only Title Only Author and Title

Blaas, N., and Humpf, H.U. (2013). Structural profiling and quantitation of glycosyl inositol phosphoceramides in plants with Fourier transform mass spectrometry. Journal of agricultural and food chemistry 61, 4257-4269.
Pubmed: Author and Title
CrossRef: Author and Title
Google Scholar: Author Only Title Only Author and Title

Borner, G.H., Sherrier, D.J., Weimar, T., Michaelson, L.V., Hawkins, N.D., Macaskill, A., Napier, J.A., Beale, M.H., Lilley, K.S., and Dupree, P. (2005). Analysis of detergent-resistant membranes in Arabidopsis. Evidence for plasma membrane lipid rafts. Plant physiology 137, 104-116.
Pubmed: Author and Title
CrossRef: Author and Title
Google Scholar: Author Only Title Only Author and Title

Brasseur, R. (1990). TAMMO: theoretical analysis of membrane molecular organisation,. In Mol. Descr. Biol. Membr. Components by Comput. Conform. Anal., (CRC Press, Boca Raton), pp. pp. 203-219.
Pubmed: Author and Title
CrossRef: Author and Title
Google Scholar: Author Only Title Only Author and Title

Bure, C., Cacas, J.L., Wang, F., Gaudin, K., Domergue, F., Mongrand, S., and Schmitter, J.M. (2011). Fast screening of highly glycosylated plant sphingolipids by tandem mass spectrometry. Rapid communications in mass spectrometry : RCM 25, 3131-3145.
Pubmed: Author and Title
CrossRef: Author and Title
Google Scholar: Author Only Title Only Author and Title

Cacas, J.L., Melser, S., Domergue, F., Joubes, J., Bourdenx, B., Schmitter, J.M., and Mongrand, S. (2012a). Rapid nanoscale quantitative analysis of plant sphingolipid long-chain bases by GC-MS. Analytical and bioanalytical chemistry 403, 2745-2755.
Pubmed: Author and Title
CrossRef: Author and Title
Google Scholar: Author Only Title Only Author and Title

Cacas, J.L., Bure, C., Furt, F., Maalouf, J.P., Badoc, A., Cluzet, S., Schmitter, J.M., Antajan, E., and Mongrand, S. (2013). Biochemical survey of the polar head of plant glycosylinositolphosphoceramides unravels broad diversity. Phytochemistry 96, 191-200.
Pubmed: Author and Title
CrossRef: Author and Title
Google Scholar: Author Only Title Only Author and Title

Cacas, J.L., Furt, F., Le Guedard, M., Schmitter, J.M., Bure, C., Gerbeau-Pissot, P., Moreau, P., Bessoule, J.J., Simon-Plas, F., and Mongrand, S. (2012b). Lipids of plant membrane rafts. Progress in lipid research 51, 272-299.
Pubmed: Author and Title
CrossRef: Author and Title
Google Scholar: Author Only Title Only Author and Title

Carmona-Salazar, L., El Hafidi, M., Gutierrez-Najera, N., Noyola-Martinez, L., Gonzalez-Solis, A., and Gavilanes-Ruiz, M. (2015). Fatty acid profiles from the plasma membrane and detergent resistant membranes of two plant species. Phytochemistry 109, 25-35.
Pubmed: Author and Title
CrossRef: Author and Title
Google Scholar: Author Only Title Only Author and Title

Carter, H.E., Gigg, R.H., Law, J.H., Nakayama, T., and Weber, E. (1958). Biochemistry of the sphingolipides. XI. Structure of phytoglycolipide. The Journal of biological chemistry 233, 1309-1314.
Pubmed: Author and Title
CrossRef: Author and Title
Google Scholar: Author Only Title Only Author and Title

Cheng, H.T., Megha, and London, E. (2009). Preparation and properties of asymmetric vesicles that mimic cell membranes: effect upon lipid raft formation and transmembrane helix orientation. The Journal of biological chemistry 284, 6079-6092.
Pubmed: Author and Title
CrossRef: Author and Title
Google Scholar: Author Only Title Only Author and Title

Deleu, M., Crowet, J.M., Nasir, M.N., and Lins, L. (2014). Complementary biophysical tools to investigate lipid specificity in the interaction between bioactive molecules and the plasma membrane: A review. Biochimica et biophysica acta 1838, 3171-3190.
Pubmed: Author and Title
CrossRef: Author and Title
Google Scholar: Author Only Title Only Author and Title

Deleu, M., Nott, K., Brasseur, R., Jacques, P., Thonart, P., and Dufrene, Y.F. (2001). Imaging mixed lipid monolayers by dynamic atomic force microscopy. Biochimica et biophysica acta 1513, 55-62.
Pubmed: Author and Title

CrossRef: Author and Title
Google Scholar: Author Only Title Only Author and Title

Devaux, P.F., and Morris, R. (2004). Transmembrane asymmetry and lateral domains in biological membranes. Traffic 5, 241-246.
Pubmed: Author and Title
CrossRef: Author and Title
Google Scholar: Author Only Title Only Author and Title

Di Paolo, G., and De Camilli, P. (2006). Phosphoinositides in cell regulation and membrane dynamics. Nature 443, 651-657.
Pubmed: Author and Title
CrossRef: Author and Title
Google Scholar: Author Only Title Only Author and Title

Ducarme, P., Rahman, M., and Brasseur, R. (1998). IMPALA: a simple restraint field to simulate the biological membrane in molecular structure studies. Proteins 30, 357-371.
Pubmed: Author and Title
CrossRef: Author and Title
Google Scholar: Author Only Title Only Author and Title

Eeman, M., Deleu, M., Paquot, M., Thonart, P., and Dufrene, Y.F. (2005). Nanoscale properties of mixed fengycin/ceramide monolayers explored using atomic force microscopy. Langmuir : the ACS journal of surfaces and colloids 21, 2505-2511.
Pubmed: Author and Title
CrossRef: Author and Title
Google Scholar: Author Only Title Only Author and Title

Eisenberg, S., Shvartsman, D.E., Ehrlich, M., and Henis, Y.I. (2006). Clustering of raft-associated proteins in the external membrane leaflet modulates internal leaflet H-ras diffusion and signaling. Molecular and cellular biology 26, 7190-7200.
Pubmed: Author and Title
CrossRef: Author and Title
Google Scholar: Author Only Title Only Author and Title

Fa, N., Lins, L., Courtoy, P.J., Dufrene, Y., Van Der Smissen, P., Brasseur, R., Tyteca, D., and Mingeot-Leclercq, M.P. (2007). Decrease of elastic moduli of DOPC bilayers induced by a macrolide antibiotic, azithromycin. Biochimica et biophysica acta 1768, 1830-1838.
Pubmed: Author and Title
CrossRef: Author and Title
Google Scholar: Author Only Title Only Author and Title

Fang, K., Zou, G., and He, P. (2003). Dynamic viscoelastic properties of spread monostearin monolayer in the presence of glycine. Journal of colloid and interface science 266, 407-414.
Pubmed: Author and Title
CrossRef: Author and Title
Google Scholar: Author Only Title Only Author and Title

Frazier, Z., and Alber, F. (2012). A computational approach to increase time scales in Brownian dynamics-based reaction-diffusion modeling. Journal of computational biology : a journal of computational molecular cell biology 19, 606-618.
Pubmed: Author and Title
CrossRef: Author and Title
Google Scholar: Author Only Title Only Author and Title

Furt, F., Simon-Plas, F., and Mongrand, S. (2011). Lipids of the plasma membrane. In The Plant Plasma Membrane. Plant Cell Monographs 19., A.S. Murphy, P. Wendy, and B. Schulz, eds (Heidelberg: Springer-Verlag), pp. 3-30.
Pubmed: Author and Title
CrossRef: Author and Title
Google Scholar: Author Only Title Only Author and Title

Furt, F., Konig, S., Bessoule, J.J., Sargueil, F., Zallot, R., Stanislas, T., Noirot, E., Lherminier, J., Simon-Plas, F., Heilmann, I., and Mongrand, S. (2010). Polyphosphoinositides are enriched in plant membrane rafts and form microdomains in the plasma membrane. Plant physiology 152, 2173-2187.
Pubmed: Author and Title
CrossRef: Author and Title
Google Scholar: Author Only Title Only Author and Title

Gaines, G.L. (1966). Insoluble Monolayers at liquid-gas Interfaces (

Garssen, M.P., van Koningsveld, R., van Doorn, P.A., Merkies, I.S., Scheltens-de Boer, M., van Leusden, J.A., van Schaik, I.N., Linssen, W.H., Visscher, F., Boon, A.M., Faber, C.G., Meulstee, J., Prick, M.J., van den Berg, L.H., Franssen, H., Hiel, J.A., van den Bergh, P.Y., and Sindic, C.J. (2007). Treatment of Guillain-Barre syndrome with mycophenolate mofetil: a pilot study. Journal of neurology, neurosurgery, and psychiatry 78, 1012-1013.
Pubmed: Author and Title
CrossRef: Author and Title
Google Scholar: Author Only Title Only Author and Title

Grosjean, K., Mongrand, S., Beney, L., Simon-Plas, F., and Gerbeau-Pissot, P. (2015). Differential effect of plant lipids on membrane organization: hot features and specificities of phytosphingolipids and phytosterols. The Journal of biological chemistry.
Pubmed: Author and Title
CrossRef: Author and Title
Google Scholar: Author Only Title Only Author and Title

Haimi, P., Uphoff, A., Hermansson, M., and Somerharju, P. (2006). Software tools for analysis of mass spectrometric lipidome data. Anal Chem 78, 8324-8331.

Pubmed: Author and Title
CrossRef: Author and Title
Google Scholar: Author Only Title Only Author and Title

Hernandez, L.E., Perotto, S., Brewin, N.J., and Drobak, B.K. (1995). A novel inositol-lipid in plant-bacteria symbiosis. Biochemical Society transactions 23, 582S.
Pubmed: Author and Title
CrossRef: Author and Title
Google Scholar: Author Only Title Only Author and Title

Jacobson, K., Mouritsen, O.G., and Anderson, R.G. (2007). Lipid rafts: at a crossroad between cell biology and physics. Nature cell biology 9, 7-14.
Pubmed: Author and Title
CrossRef: Author and Title
Google Scholar: Author Only Title Only Author and Title

Jarsch, I.K., Konrad, S.S., Stratil, T.F., Urbanus, S.L., Szymanski, W., Braun, P., Braun, K.H., and Ott, T. (2014). Plasma Membranes Are Subcompartmentalized into a Plethora of Coexisting and Diverse Microdomains in Arabidopsis and Nicotiana benthamiana. The Plant cell 26, 1698-1711.
Pubmed: Author and Title
CrossRef: Author and Title
Google Scholar: Author Only Title Only Author and Title

Kaul, K., and Lester, R.L. (1975). Characterization of Inositol-containing Phosphosphingolipids from Tobacco Leaves: Isolation and Identification of Two Novel, Major Lipids: N-Acetylglucosamidoglucuronidoinositol Phosphorylceramide and Glucosamidoglucuronidoinositol Phosphorylceramide. Plant physiology 55, 120-129.
Pubmed: Author and Title
CrossRef: Author and Title
Google Scholar: Author Only Title Only Author and Title

Lefebvre, B., Furt, F., Hartmann, M.A., Michaelson, L.V., Carde, J.P., Sargueil-Boiron, F., Rossignol, M., Napier, J.A., Cullimore, J., Bessoule, J.J., and Mongrand, S. (2007). Characterization of lipid rafts from Medicago truncatula root plasma membranes: a proteomic study reveals the presence of a raft-associated redox system. Plant physiology 144, 402-418.
Pubmed: Author and Title
CrossRef: Author and Title
Google Scholar: Author Only Title Only Author and Title

Lins, L., and Brasseur, R. (1995). The hydrophobic effect in protein folding. FASEB journal : official publication of the Federation of American Societies for Experimental Biology 9, 535-540.
Pubmed: Author and Title
CrossRef: Author and Title
Google Scholar: Author Only Title Only Author and Title

Lins, L., Charloteaux, B., Thomas, A., and Brasseur, R. (2001). Computational study of lipid-destabilizing protein fragments: towards a comprehensive view of tilted peptides. Proteins 44, 435-447.
Pubmed: Author and Title
CrossRef: Author and Title
Google Scholar: Author Only Title Only Author and Title

Lins, L., Brasseur, R., Malaisse, W.J., Biesemans, M., Verheyden, P., and Willem, R. (1996). Importance of the hydrophobic energy: structural determination of a hypoglycemic drug of the meglitinide family by nuclear magnetic resonance and molecular modeling. Biochemical pharmacology 52, 1155-1168.
Pubmed: Author and Title
CrossRef: Author and Title
Google Scholar: Author Only Title Only Author and Title

Lins, L., Thomas-Soumarmon, A., Pillot, T., Vandekerchkhove, J., Rosseneu, M., and Brasseur, R. (1999). Molecular determinants of the interaction between the C-terminal domain of Alzheimer's beta-amyloid peptide and apolipoprotein E alpha-helices. Journal of neurochemistry 73, 758-769.
Pubmed: Author and Title
CrossRef: Author and Title
Google Scholar: Author Only Title Only Author and Title

Maget-Dana, R. (1999). The monolayer technique: a potent tool for studying the interfacial properties of antimicrobial and membrane-lytic peptides and their interactions with lipid membranes. Biochimica et biophysica acta 1462, 109-140.
Pubmed: Author and Title
CrossRef: Author and Title
Google Scholar: Author Only Title Only Author and Title

Markham, J.E., Li, J., Cahoon, E.B., and Jaworski, J.G. (2006). Separation and identification of major plant sphingolipid classes from leaves. The Journal of biological chemistry 281, 22684-22694.
Pubmed: Author and Title
CrossRef: Author and Title
Google Scholar: Author Only Title Only Author and Title

Martiniere, A., Lavagi, I., Nageswaran, G., Rolfe, D.J., Maneta-Peyret, L., Luu, D.T., Botchway, S.W., Webb, S.E., Mongrand, S., Maurel, C., Martin-Fernandez, M.L., Kleine-Vehn, J., Friml, J., Moreau, P., and Runions, J. (2012). Cell wall constrains lateral diffusion of plant plasma-membrane proteins. Proceedings of the National Academy of Sciences of the United States of America 109, 12805-12810.
Pubmed: Author and Title

CrossRef: Author and Title
Google Scholar: Author Only Title Only Author and Title

Masserini, M., Palestini, P., and Freire, E. (1989). Influence of glycolipid oligosaccharide and long-chain base composition on the thermotropic properties of dipalmitoylphosphatidylcholine large unilamellar vesicles containing gangliosides. Biochemistry 28, 5029-5034.
Pubmed: Author and Title
CrossRef: Author and Title
Google Scholar: Author Only Title Only Author and Title

Matyash, V., Liebisch, G., Kurzchalia, T.V., Shevchenko, A., and Schwudke, D. (2008). Lipid extraction by methyl-tert-butyl ether for high-throughput lipidomics. Journal of lipid research 49, 1137-1146.
Pubmed: Author and Title
CrossRef: Author and Title
Google Scholar: Author Only Title Only Author and Title

Mongrand, S., Stanislas, T., Bayer, E.M., Lherminier, J., and Simon-Plas, F. (2010). Membrane rafts in plant cells. Trends in plant science 15, 656-663.
Pubmed: Author and Title
CrossRef: Author and Title
Google Scholar: Author Only Title Only Author and Title

Mongrand, S., Morel, J., Laroche, J., Claverol, S., Carde, J.P., Hartmann, M.A, Bonneu, M., Simon-Plas, F., Lessire, R., and Bessoule, J.J. (2004). Lipid rafts in higher plant cells: purification and characterization of Triton X-100-insoluble microdomains from tobacco plasma membrane. The Journal of biological chemistry 279, 36277-36286.
Pubmed: Author and Title
CrossRef: Author and Title
Google Scholar: Author Only Title Only Author and Title

Morel, J., Claverol, S., Mongrand, S., Furt, F., Fromentin, J., Bessoule, J.J., Blein, J.P., and Simon-Plas, F. (2006). Proteomics of plant detergent-resistant membranes. Molecular & cellular proteomics : MCP 5, 1396-1411.
Pubmed: Author and Title
CrossRef: Author and Title
Google Scholar: Author Only Title Only Author and Title

Mortimer, J.C., Yu, X., Albrecht, S., Sicilia, F., Huichalaf, M., Ampuero, D., Michaelson, L.V., Murphy, A.M., Matsunaga, T., Kurz, S., Stephens, E., Baldwin, T.C., Ishii, T., Napier, J.A., Weber, A.P., Handford, M.G., and Dupree, P. (2013). Abnormal glycosphingolipid mannosylation triggers salicylic acid-mediated responses in Arabidopsis. The Plant cell 25, 1881-1894.
Pubmed: Author and Title
CrossRef: Author and Title
Google Scholar: Author Only Title Only Author and Title

Mouritsen, O.G. (2010). The liquid-ordered state comes of age. Biochimica et biophysica acta 1798, 1286-1288.
Pubmed: Author and Title
CrossRef: Author and Title
Google Scholar: Author Only Title Only Author and Title

Noirot, E., Der, C., Lherminier, J., Robert, F., Moricova, P., Kieu, K., Leborgne-Castel, N., Simon-Plas, F., and Bouhidel, K. (2014). Dynamic changes in the subcellular distribution of the tobacco ROS-producing enzyme RBOHD in response to the oomycete elicitor cryptogein. Journal of experimental botany 65, 5011-5022.
Pubmed: Author and Title
CrossRef: Author and Title
Google Scholar: Author Only Title Only Author and Title

Pascher, I. (1976). Molecular arrangements in sphingolipids. Conformation and hydrogen bonding of ceramide and their implication on membrane stability and permeability. Biochimica et biophysica acta 455, 433-451.
Pubmed: Author and Title
CrossRef: Author and Title
Google Scholar: Author Only Title Only Author and Title

Pata, M.O., Hannun, Y.A., and Ng, C.K. (2010). Plant sphingolipids: decoding the enigma of the Sphinx. The New phytologist 185, 611-630.
Pubmed: Author and Title
CrossRef: Author and Title
Google Scholar: Author Only Title Only Author and Title

Quinn, P.J., and Wolf, C. (2009). The liquid-ordered phase in membranes. Biochimica et biophysica acta 1788, 33-46.
Pubmed: Author and Title
CrossRef: Author and Title
Google Scholar: Author Only Title Only Author and Title

Raffaele, S., Bayer, E., Lafarge, D., Cluzet, S., German Retana, S., Boubekeur, T., Leborgne-Castel, N., Carde, J.P., Lherminier, J., Noirot, E., Satiat-Jeunemaitre, B., Laroche-Traineau, J., Moreau, P., Ott, T., Maule, A.J., Reymond, P., Simon-Plas, F., Farmer, E.E., Bessoule, J.J., and Mongrand, S. (2009). Remorin, a solanaceae protein resident in membrane rafts and plasmodesmata, impairs potato virus X movement. The Plant cell 21, 1541-1555.
Pubmed: Author and Title
CrossRef: Author and Title
Google Scholar: Author Only Title Only Author and Title

Rehman, R.U., Stigliano, E., Lycett, G.W., Sticher, L., Sbano, F., Faraco, M., Dalessandro, G., and Di Sansebastiano, G.P. (2008).

Tomato Rab11a characterization evidenced a difference between SYP121-dependent and SYP122-dependent exocytosis. Plant Cell Physiol 49, 751-766.
Pubmed: Author and Title
CrossRef: Author and Title
Google Scholar: Author Only Title Only Author and Title

Rennie, E.A., Ebert, B., Miles, G.P., Cahoon, R.E., Christiansen, K.M., Stonebloom, S., Khatab, H., Twell, D., Petzold, C.J., Adams, P.D., Dupree, P., Heazlewood, J.L., Cahoon, E.B., and Scheller, H.V. (2014). Identification of a sphingolipid alpha-glucuronosyltransferase that is essential for pollen function in Arabidopsis. The Plant cell 26, 3314-3325.
Pubmed: Author and Title
CrossRef: Author and Title
Google Scholar: Author Only Title Only Author and Title

Richards, R.L., Rao, M., Wassef, N.M., Glenn, G.M., Rothwell, S.W., and Alving, C.R. (1998). Liposomes containing lipid A serve as an adjuvant for induction of antibody and cytotoxic T-cell responses against RTS,S malaria antigen. Infection and immunity 66, 2859-2865.
Pubmed: Author and Title
CrossRef: Author and Title
Google Scholar: Author Only Title Only Author and Title

Rideal, J.T.D.a.E.K. (1963). Interfacial Phenomena (

Ripley, B.D. (1976). The second order analysis of stationary point process. Journal of Applied Probability 13, 255-261.
Pubmed: Author and Title
CrossRef: Author and Title
Google Scholar: Author Only Title Only Author and Title

Ruettinger, A., Kiselev, M.A., Hauss, T., Dante, S., Balagurov, A.M., and Neubert, R.H. (2008). Fatty acid interdigitation in stratum corneum model membranes: a neutron diffraction study. European biophysics journal : EBJ 37, 759-771.
Pubmed: Author and Title
CrossRef: Author and Title
Google Scholar: Author Only Title Only Author and Title

Scheffer, L., Solomonov, I., Weygand, M.J., Kjaer, K., Leiserowitz, L., and Addadi, L. (2005). Structure of cholesterol/ceramide monolayer mixtures: implications to the molecular organization of lipid rafts. Biophysical journal 88, 3381-3391.
Pubmed: Author and Title
CrossRef: Author and Title
Google Scholar: Author Only Title Only Author and Title

Shevchenko, A., and Simons, K. (2010). Lipidomics: coming to grips with lipid diversity. Nature reviews. Molecular cell biology 11, 593-598.
Pubmed: Author and Title
CrossRef: Author and Title
Google Scholar: Author Only Title Only Author and Title

Simon-Plas, F., Perraki, A., Bayer, E., Gerbeau-Pissot, P., and Mongrand, S. (2011). An update on plant membrane rafts. Current opinion in plant biology 14, 642-649.
Pubmed: Author and Title
CrossRef: Author and Title
Google Scholar: Author Only Title Only Author and Title

Simons, K., and Ikonen, E. (1997). Functional rafts in cell membranes. Nature 387, 569-572.
Pubmed: Author and Title
CrossRef: Author and Title
Google Scholar: Author Only Title Only Author and Title

Simons, K., and Toomre, D. (2000). Lipid rafts and signal transduction. Nature reviews. Molecular cell biology 1, 31-39.
Pubmed: Author and Title
CrossRef: Author and Title
Google Scholar: Author Only Title Only Author and Title

Simons, K., and Gerl, M.J. (2010). Revitalizing membrane rafts: new tools and insights. Nature reviews. Molecular cell biology 11, 688-699.
Pubmed: Author and Title
CrossRef: Author and Title
Google Scholar: Author Only Title Only Author and Title

Sonnino, S., and Prinetti, A. (2010). Gangliosides as regulators of cell membrane organization and functions. Advances in experimental medicine and biology 688, 165-184.
Pubmed: Author and Title
CrossRef: Author and Title
Google Scholar: Author Only Title Only Author and Title

Sperling, P., and Heinz, E. (2003). Plant sphingolipids: structural diversity, biosynthesis, first genes and functions. Biochimica et biophysica acta 1632, 1-15.
Pubmed: Author and Title
CrossRef: Author and Title
Google Scholar: Author Only Title Only Author and Title

Sperling, P., Franke, S., Luthje, S., and Heinz, E. (2005). Are glucocerebrosides the predominant sphingolipids in plant plasma membranes? Plant Physiol Biochem 43, 1031-1038.

Pubmed: Author and Title
CrossRef: Author and Title
Google Scholar: Author Only Title Only Author and Title

Subczynski, W.K., and Kusumi, A. (2003). Dynamics of raft molecules in the cell and artificial membranes: approaches by pulse EPR spin labeling and single molecule optical microscopy. Biochimica et biophysica acta 1610, 231-243.
Pubmed: Author and Title
CrossRef: Author and Title
Google Scholar: Author Only Title Only Author and Title

Tjellstrom, H., Hellgren, L.I., Wieslander, A., and Sandelius, A.S. (2010). Lipid asymmetry in plant plasma membranes: phosphate deficiency-induced phospholipid replacement is restricted to the cytosolic leaflet. FASEB journal : official publication of the Federation of American Societies for Experimental Biology 24, 1128-1138.
Pubmed: Author and Title
CrossRef: Author and Title
Google Scholar: Author Only Title Only Author and Title

Vitiello, F., and Zanetta, J.P. (1978). Thin-layer chromatography of phospholipids. Journal of chromatography 166, 637-640.
Pubmed: Author and Title
CrossRef: Author and Title
Google Scholar: Author Only Title Only Author and Title

Voxeur, A., and Fry, S.C. (2014). Glycosylinositol phosphorylceramides from Rosa cell cultures are boron-bridged in the plasma membrane and form complexes with rhamnogalacturonan II. The Plant journal : for cell and molecular biology 79, 139-149.
Pubmed: Author and Title
CrossRef: Author and Title
Google Scholar: Author Only Title Only Author and Title

Wang, W., Yang, X., Tangchaiburana, S., Ndeh, R., Markham, J.E., Tsegaye, Y., Dunn, T.M., Wang, G.L., Bellizzi, M., Parsons, J.F., Morrissey, D., Bravo, J.E., Lynch, D.V., and Xiao, S. (2008). An inositolphosphorylceramide synthase is involved in regulation of plant programmed cell death associated with defense in Arabidopsis. The Plant cell 20, 3163-3179.
Pubmed: Author and Title
CrossRef: Author and Title
Google Scholar: Author Only Title Only Author and Title

Worrall, D., Ng, C.K., and Hetherington, A.M. (2003). Sphingolipids, new players in plant signaling. Trends in plant science 8, 317-320.
Pubmed: Author and Title
CrossRef: Author and Title
Google Scholar: Author Only Title Only Author and Title

Yetukuri, L., Ekroos, K., Vidal-Puig, A., and Oresic, M. (2008). Informatics and computational strategies for the study of lipids. Molecular bioSystems 4, 121-127.
Pubmed: Author and Title
CrossRef: Author and Title
Google Scholar: Author Only Title Only Author and Title